CHAPTER 3

RESULTS AND DISCUSSION

CHAPTER 3

RESULTS AND DISCUSSION

3.1. Preparation and choice of the uranium target:

3.1.1. Target wrapper and irradiation can:

The target wrappers and the irradiation cans were made of the highest- purity aluminum products because of the following reasons:

1. Amount of energy released from the fission process is ~200 MeV for each fission event. The high thermal conductivity of aluminum (2.37 W/cmK) enhances the dissipation of heat accompanying the fission process during irradiation.
2. ^{28}Al isotope, which was produced during target irradiation via the nuclear reaction $^{27}Al(n,\gamma)^{28}Al$, is a short-lived isotope ($T_{1/2}$ = 2.25 min) so that no radioactivity due to ^{28}Al (E_γ = 1779 keV) was detected in the irradiated targets and their solutes after the cooling period.
3. The aluminum wrappers were suitable for direct introduction of the irradiated uranium target to chemical processing. The aluminum wrapper, containing the irradiated uranium target, was dissolved in the digesting agent, NaOH solution, to avoid any loss of the irradiated target, contaminating the surrounding atmosphere, disbatch operations, and radiation hazards.
4. Aluminum is available in high-purity with reasonable prices.

In case of weights higher than 0.02 g of the target (i.e., 0.06 and 0.1 g), it was recommended to fill the inner space of the irradiation can with thin aluminum foils for further enhancement of heat dissipation avoiding any problems of heat accumulation in the can during irradiation.

3.1.2. Uranium targets:

The uranium targets were irradiated at a thermal neutron flux of 1×10^{14} n/cm^{2}s in the ETRR-2 Egypt Research Reactor. The average ratio of fast neutrons to thermal neutrons, n_f / n_{th}, in the irradiation positions is ~0.55 at beginning of the fuel cycle and ~0.52 at end of it. Figure 3.1 (a and b) shows the gamma spectra of the UO_3 target before and after irradiation for 4 h and cooling for one week. Figure 3.1(a) shows the γ-photopeaks of ^{235}U, ^{238}U, and ^{234m}Pa appeared in the gamma spectrum of the UO_3 target before irradiation. Figure 3.1 (b) shows the γ-photopeaks of ^{95}Zr, ^{97}Zr, ^{95}Nb, ^{97m}Nb, $^{99}Mo/^{99m}Tc$, ^{103}Ru, ^{132}Te, ^{131}I, ^{132}I, $^{137}Cs/^{137m}Ba$, ^{140}Ba, ^{140}La, ^{141}Ce, ^{238}U, ^{235}U, and ^{239}Np appeared in the gamma spectrum of the UO_3 after irradiation. Many other radioisotopes (such as ^{125m}Te, ^{129}I, ^{89}Sr, ^{136}Cs, ^{141}Cs, ^{142}Cs, ^{101}Mo, and ^{102}Mo) did not appear in the gamma spectrum of the irradiated target because of one or more of the following reasons: (i) low fission yield, (ii) low-energy or low-abundance gamma rays, (iii) interferences between γ-photopeaks due to presence of many isotopes with converging characteristic values of decay-gamma ray energies, and (iv) absence of gamma-ray emission. Generally, some of these radioisotopes were successfully appeared, where the interference and overlap of the different γ-photopeaks would decrease with the successive separation processes. Fission yields of the isotopes mentioned in this work were cited from **Etherington (1958)** and **England and Rider (1993)**, whereas the half-lives and decay data of the radioactive isotopes were cited from **Burrows (1988)** and **Chu et al. (1999)**.

Preliminary irradiation processes were conducted using uranyl nitrate hexahydrate targets. During irradiation of the uranyl nitrate targets, tritium (^3H) may be produced as a result of bombarding nitrogen atoms of the

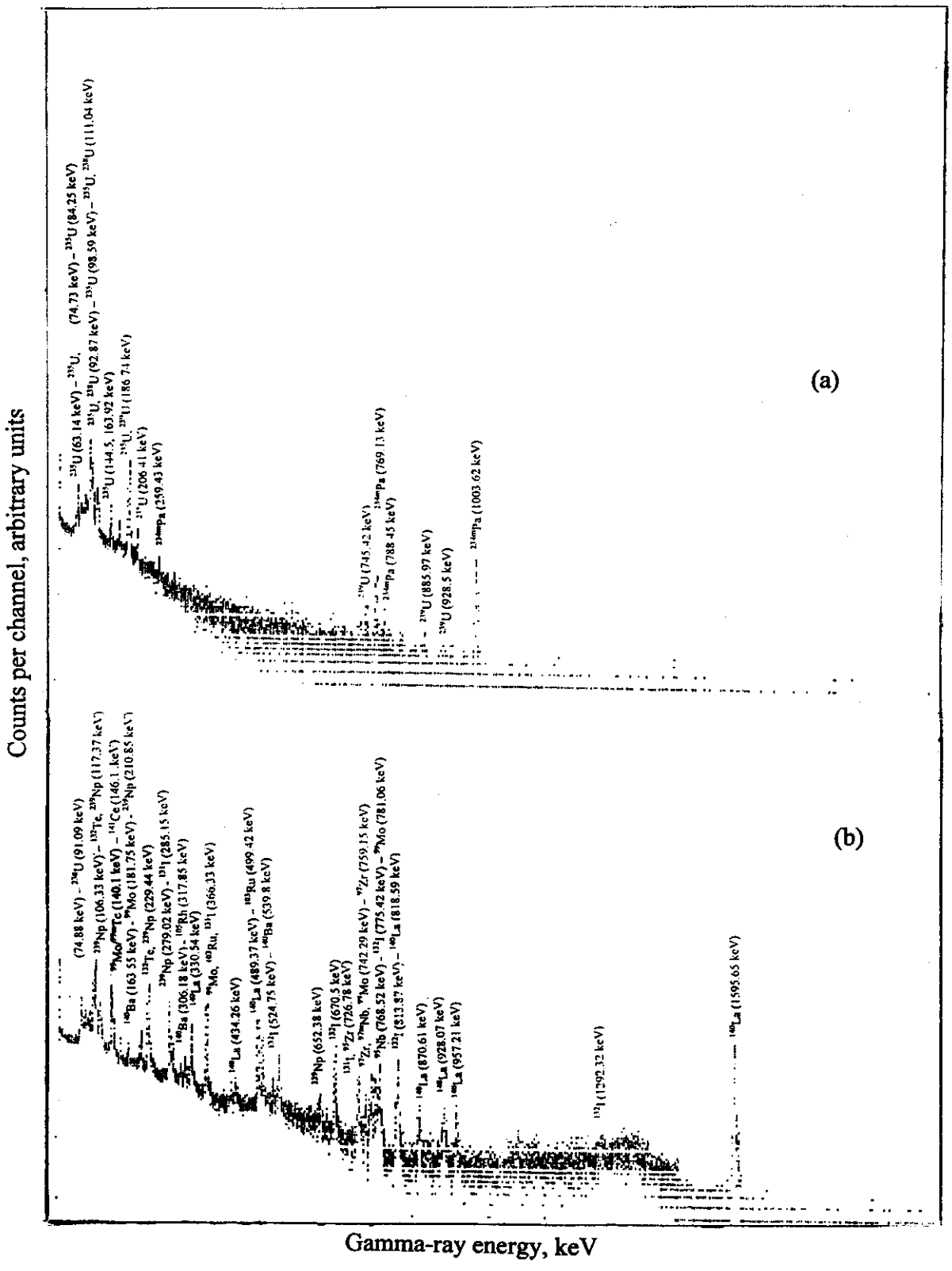

Figure 3.1. Gamma spectra of the UO_3 target (a) before irradiation and (b) after irradiation for 4 h at a thermal neutron flux of 1×10^{14} n/cm^{2}s and cooling for one week.

nitrate group by fast neutrons according to the following reaction **(Choppin and Rydberg, 1980)**:

$$^{1}_{0}n(fast) + {}^{14}N \longrightarrow {}^{12}C + {}^{3}H$$

According to the previous equation, fast neutron irradiation of uranyl nitrate would increase the tritium content (where tritium is also produced as a fission product, independent of chemical structure of the uranium target, in small mass quantities of $\sim 2.8 \times 10^{-5}$ g tritium/kg nuclear fuel) **(Bray et al., 1981)**. Although tritium ($T_{1/2}$ = 12.32 y) emits relatively low-energy beta particles (5.69 keV), it has many hazardous effects on health and environment **(Straume, 1991; DOE, 1995)**. On the other hand, protium (^{1}H) was produced during irradiation of the uranyl nitrate by bombarding nitrogen atoms of the nitrate group with slow neutrons according to **(Choppin and Rydberg, 1980)**:

$$^{1}_{0}n(slow) + {}^{14}N \longrightarrow {}^{14}C + {}^{1}H$$

Between 200 and 350°C, uranyl nitrate hexahydrate undergoes thermal decomposition resulting in formation of NO_2 and O_2 gases, and water vapor according to the following equation **(Cordfunke, 1969)**:

$$UO_2(NO_3)_2.6H_2O \xrightarrow{200\text{-}350^{\circ}C} UO_3 + 2NO_2 + 1/2O_2 + 6H_2O_{(g)}$$

All these gases (^{3}H, ^{1}H, NO_2, O_2) and water vapor, produced during irradiation of the uranyl nitrate hexahydrate target, would increase the pressure inside the aluminum wrapper and, consequently, inside the irradiation can which may cause adverse effects during the irradiation,

cooling, and decanning processes. On the other hand, in case of uranium trioxide, the following thermal decomposition reaction may occur during its irradiation **(Cotton and Wilkinson, 1979)**:

$$3UO_3 \xrightarrow{700°C} U_3O_8 + \tfrac{1}{2}O_2$$

However, uranyl nitrate targets have a high solubility in organic liquids which found practical importance in solvent extraction applications **(Cordfunke, 1969)**. UO_3 was preferred as a target material, where lower amounts of gases are produced during irradiation than in case of $UO_3(NO_3)_2.6H_2O$. The uranyl nitrate hexahydrate target was used in the preliminary experiments of this work to establish a standard processing procedure. Thereafter, UO_3 targets were used in different weights (0.02, 0.06, and 0.1 g).

3.2. Digestion of the irradiated uranium targets:

At end of the seven-days cooling period, the irradiated uranium target was digested in a sodium hydroxide solution.

3.2.1. Advantages of alkali digestion over acid dissolution:

There are three main advantages for alkali digestion of the irradiated uranium targets which are not present in case of acid dissolution; these are **(Vandegrift et al., 1997)**:

1. Digestion in the alkali solution releases the noble fission gases (krypton and xenon), while radioiodine remains in the fission-products solution, i.e., noble fission gases can be recovered separately from radioiodine.
2. On lowering pH-value of the fission-products solution, radioiodine releases in the gas phase allowing its separate recovery.

3. The digestion in the alkali solution causes the precipitation of the uranium bulk as uranate (or diuranate), and many other fission products as insoluble hydroxides. This is considered as a decontamination step in the chemical processing to recover one or more desired fission isotope.

3.2.2. The digestion technique:

Figure 3.2 (a and b) shows the gamma spectra of the supernatant and the residue obtained from digestion of the irradiated UO_3 target in 10 ml of 2 M NaOH solution for ~12 h. Figure 3.2 indicates that the radioisotopes distributed themselves between the supernatant and the residue as follows:

1. $^{137}Cs/^{137m}Ba$ and $^{99}Mo/^{99m}Tc$ were completely included in the supernatant.
2. Bulk of the uranium target, ^{238}U and ^{235}U, was included in the residue.
3. The other radioisotopes distributed themselves between the supernatant and the residue with different ratios.

The aluminum wrapper dissolves in the sodium hydroxide solution forming sodium aluminate according to the following equation **(Foster et al., 1955)**:

$$Al + NaOH + H_2O \longrightarrow NaAlO_2 + 3/2H_2$$

Though it is likely that the species in the solution is the hydrated tetrahydroxoaluminate anion $[Al(OH)_4]^-_{(aq)}$ or $[Al(H_2O)_2(OH)_4]^-_{(aq)}$ **(Greenwood and Earnshaw, 1984)**. Both of the uranyl nitrate and the uranium trioxide targets react with NaOH solution producing sodium uranate precipitate, Na_2UO_4, (which commonly encountered as sodium diuranate, $Na_2U_2O_7$) according to the following equations:

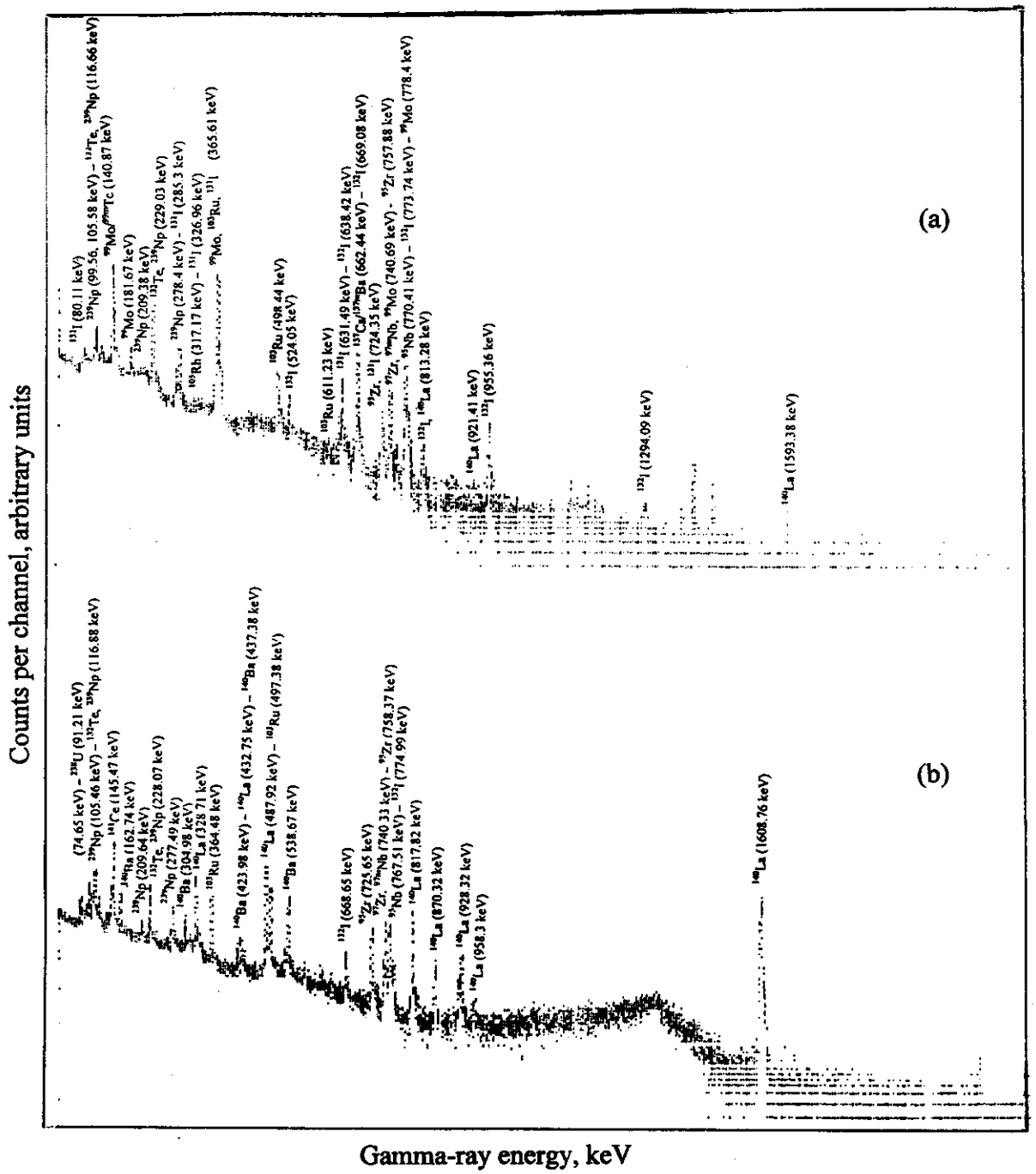

Figure 3.2. Gamma spectra of (a) the supernatant and (b) the residue obtained from the digestion process of the thermal neutron irradiated UO_3 target in NaOH solution.

$$UO_2(NO_3)_2.6H_2O + 4NaOH \longrightarrow Na_2UO_4\downarrow + 2NaNO_3 + 8H_2O$$

or

$$2UO_2(NO_3)_2.6H_2O + 6NaOH \longrightarrow Na_2U_2O_7\downarrow + 4NaNO_3 + 15H_2O$$

$$UO_3 + 2NaOH \longrightarrow Na_2UO_4\downarrow + H_2O$$

or

$$2UO_3 + 2NaOH \longrightarrow Na_2U_2O_7\downarrow + H_2O$$

At beginning of the digestion process, the aluminum wrapper containing the irradiated uranium target was introduced to the three-nick bottle of the digestion system (Figure 2.1) together with the digesting agent (10 ml of 2 M NaOH). Thereafter, a current of air was introduced to the three-nick bottle and withdrawn by a pump to carry the fission gases (tritium, krypton, xenon, and a fraction of iodine) which were expected to escape during digestion and the gases produced as a result of the digestion reactions, such as hydrogen obtained from reaction of aluminum wrapper with NaOH solution, or during the irradiation, such as O_2 in case of UO_3 or NO_2, protium, and tritium in case of the uranyl nitrate. The stream of gases passed through an alkali trap (15 ml of 3 M NaOH) to retain NO_2 and I_2, and then passed through a nitrogen-cooled filter containing activated charcoal impregnated with silver nitrate solution to absorb krypton and xenon gases, and also any traces of iodine escaping from the alkali trap. Finally, the gaseous stream passed through the pump to ventilation. After ~12 h, the supernatant was withdrawn and centrifuged to ensure that it became free from any traces of the uranate (or diuranate) residue.

Figure 3.3 (a and b) shows the gamma spectra of the alkali trap (in which ^{131}I appeared) and of the charcoal filter (in which traces of ^{131}I and ^{133}Xe appeared) of the digestion system. Fission reactions of ^{235}U produce

21 xenon isotopes; ^{129}Xe, ^{131m}Xe, ^{131}Xe, ^{132}Xe, ^{133m}Xe, ^{133}Xe, ^{134m}Xe, ^{134}Xe, ^{135m}Xe, ^{135}Xe, ^{136}Xe, ^{137}Xe, ^{138}Xe, ^{139}Xe, ^{140}Xe, ^{141}Xe, ^{142}Xe, ^{143}Xe, ^{144}Xe, ^{145}Xe, and ^{146}Xe. Five of these isotopes are stable nuclides while the other are radioactive ones. The five stable ones are ^{129}Xe, ^{131}Xe, ^{132}Xe, ^{134}Xe, and ^{136}Xe. There are 13 short-lived fission-xenon isotopes with half-lives ranging from a fraction of second to few hours; ^{134m}Xe ($T_{1/2}$ = 0.29 s), ^{135m}Xe ($T_{1/2}$ = 15.36 min), ^{135}Xe ($T_{1/2}$ = 9.1 h), ^{137}Xe ($T_{1/2}$ = 3.82 min), ^{138}Xe ($T_{1/2}$ = 14.13 min), ^{139}Xe ($T_{1/2}$ = 39.68 s), ^{140}Xe ($T_{1/2}$ = 13.6 s), ^{141}Xe ($T_{1/2}$ = 1.73 s), ^{142}Xe ($T_{1/2}$ = 1.22 s), ^{143}Xe ($T_{1/2}$ = 0.3 s), ^{144}Xe ($T_{1/2}$ = 1.15 s), ^{145}Xe ($T_{1/2}$ = 0.9 s), and ^{146}Xe ($T_{1/2}$ = 0.56 s). These short-lived xenon isotopes decayed practically, completely during the seven-days cooling period. There are three fission-xenon isotopes with half-lives in the order of few days; ^{131m}Xe ($T_{1/2}$ = 11.9 d), ^{133m}Xe ($T_{1/2}$ = 2.19 d), ^{133}Xe ($T_{1/2}$ = 5.24 d). ^{131m}Xe and ^{133m}Xe have (i) low fission yields (0.034 and 0.192 %, respectively), and (ii) low-abundance gamma rays (1.7 % of 163.97 keV and 9.9 % of 233.5 keV, respectively). Among the fission-xenon isotopes, only ^{133}Xe was detected in the gamma spectrum of the charcoal filter of the digestion system, as shown in Figure 3.3 (b). This is because of its (i) suitable half-life, (ii) high fission yield (Y_f = 6.7 %), and (iii) measurable energy of gamma rays of decay (36.6 % of 80.99 keV).

^{235}U-fission reactions produce 18 krypton isotopes; ^{82}Kr, ^{83m}Kr, ^{83}Kr, ^{84}Kr, ^{85m}Kr, ^{85}Kr, ^{86}Kr, ^{87}Kr, ^{88}Kr, ^{89}Kr, ^{90}Kr, ^{91}Kr, ^{92}Kr, ^{93}Kr, and ^{94}Kr. Of these isotopes, there are four stable ones; ^{82}Kr, ^{83}Kr, ^{84}Kr, and ^{86}Kr. There are 13 short-lived fission-krypton isotopes with half-lives ranging from a fraction of second to few hours; ^{83m}Kr ($T_{1/2}$ = 1.86 h), ^{85m}Kr ($T_{1/2}$ = 4.48 h) ^{87}Kr ($T_{1/2}$ = 1.27 h), ^{88}Kr ($T_{1/2}$ = 2.84 h), ^{89}Kr ($T_{1/2}$ = 3.15 min), ^{90}Kr ($T_{1/2}$ = 32.3 s), ^{91}Kr ($T_{1/2}$ = 8.57 s), ^{92}Kr ($T_{1/2}$ = 1.84 s), ^{93}Kr ($T_{1/2}$ = 1.29 s), ^{94}Kr ($T_{1/2}$ = 0.2 s), ^{95}Kr ($T_{1/2}$ = 0.78 s), ^{96}Kr ($T_{1/2}$ = 0.29 s), and ^{97}Kr ($T_{1/2}$ = 0.1 s). All of these short-lived krypton isotopes decayed practically,

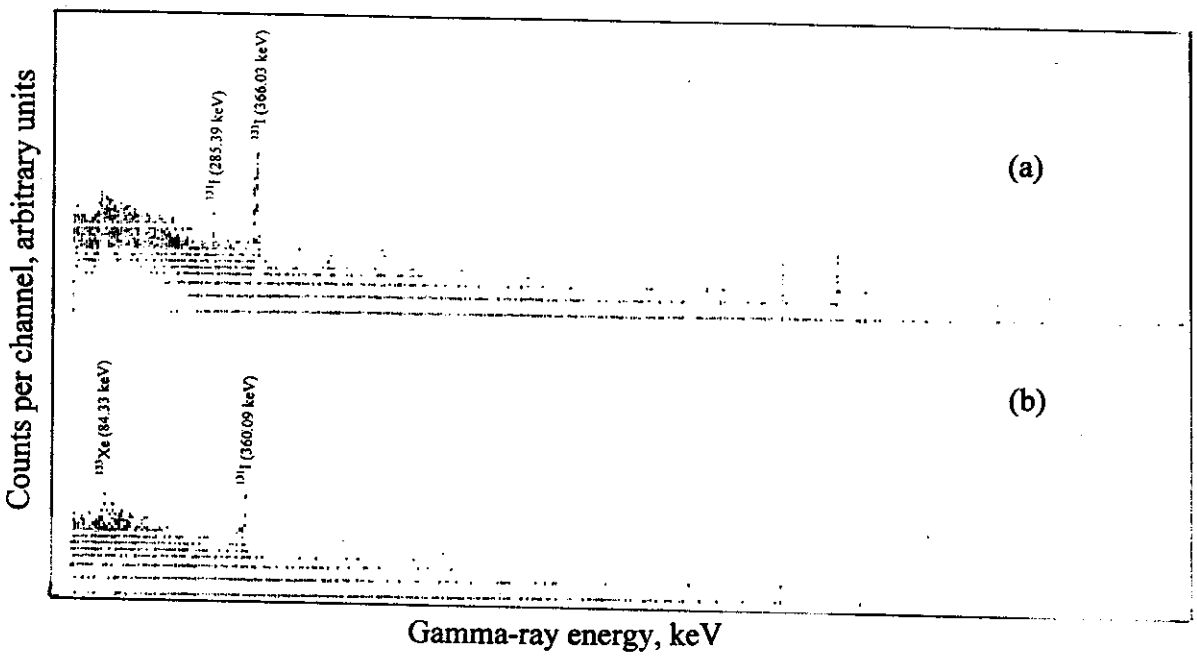

Figure 3.3. Gamma spectra of the (a) alkali trap and (b) charcoal filter of the digestion system.

completely during the cooling time of seven days. The only long-lived fission-krypton isotope is ^{85}Kr ($T_{1/2}$ = 10.73 y). Krypton-85 is of low importance because: (i) it has a low fission yield (Y_f = 0.283 %), and (ii) it has low-abundance gamma rays of decay (0.4 % of 513.97 keV). Thus, none of krypton radioisotopes appeared in the gamma spectrum of the charcoal filter (Figure 3.3, b) because of their short half-lives, low fission yields, and/or low-abundance gamma rays of decay. Figure 3.4 (a and b) shows the decay chains of ^{85}Kr and ^{133}Xe as ^{235}U-fission products, while Table 3.1 compiles the nuclear characteristics and fission yields of the krypton and xenon isotopes produced from fission reactions of ^{235}U.

The iodine isotopes that are produced from the fission of ^{235}U will be mentioned latter in details (Section 3.2).

3.2. Production of radioiodine:

Figure 3.1 (b) indicates presence of the γ-photopeaks of ^{131}I (366.33, 285.15, and 726.78 keV), ^{132}I (670.5, 524.75, 775.42, 813.87, and 1292.32 keV), and ^{132}Te (229.44 and 117.37 keV). Fission reactions of ^{235}U give rise to 11 iodine isotopes; ^{127}I, ^{129}I, ^{131}I, ^{132}I, ^{133}I, ^{134}I, ^{135}I, ^{136}I, ^{137}I, ^{138}I, and ^{139}I. Iodine-127 is stable, whereas ^{134}I, ^{135}I, ^{136}I, ^{137}I, ^{138}I, and ^{139}I are short-lived radioisotopes with half-life periods of 52.6 min, 6.57 h, 1.39 min, 24.5 s, 6.49 s, and 2.28 s, respectively, so that they decayed completely during the seven-days cooling period. Iodine-133 ($T_{1/2}$ = 20.8 h) did not appear in any of the gamma spectra of this work as a result of its relatively-short half-life and, generally, the sweep of its decay products ^{133m}Xe and ^{133}Xe during irradiation and cooling of the uranium targets. Iodine-129 ($T_{1/2}$ = 1.57 × 10^7 y), which decays to stable ^{129}Xe, did not appear in the gamma spectra because of its low-energy gamma rays (29.78 keV). The most important ^{235}U fission-iodine isotopes are ^{131}I ($T_{1/2}$ = 8.04 d) and

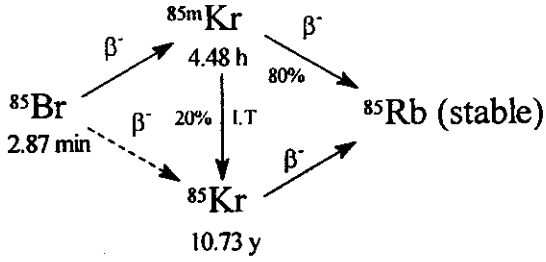

(a)

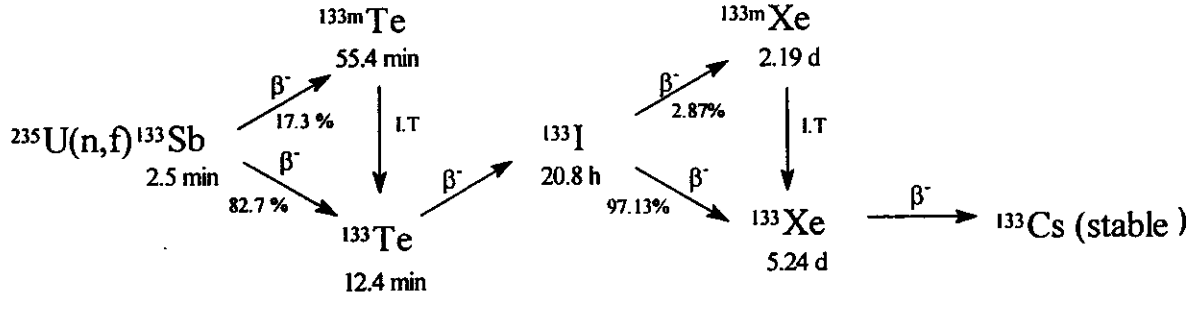

(b)

Figure 3.4. Decay chains of (a) ^{85}Kr and (b) ^{133}Xe as ^{235}U-fission products.

Table 3.1. Nuclear characteristics and fission yields of the ^{235}U-fission krypton and xenon isotopes.

Isotope		Half-life, $T_{1/2}$	Fission yield, Y_f	Decay mode	Main γ-energy (abundance), and other γ-energies in keV
Krypton isotopes	^{82}Kr	Stable	3.5×10^{-5} %	-	-
	^{83m}Kr	1.86 h	0.536 %	I.T	9.4 (5.4 %), 32.15
	^{83}Kr	Stable	0.536 %	-	-
	^{84}Kr	Stable	1.1 %	-	-
	^{85m}Kr	4.48 h	1.29 %	β^-, I.T	151.8 (75.3 %), 129.85, 304.87, ...
	^{85}Kr	10.73 y	0.283 %	β^-	513.97 (0.4 %), 151.16, 362.81, ...
	^{86}Kr	Stable	2.1 %	-	-
	^{87}Kr	1.27 h	2.56 %	β^-	402.58 (49.5 %), 2554.8, 845.43, ...
	^{88}Kr	2.84 h	3.55 %	β^-	2392.11 (34.6 %), 196.32, 2195.84, ...
	^{89}Kr	3.15 min	4.51 %	β^-	220.9 (20 %), 585.5, 904.27, ...
	^{90}Kr	32.3 s	4.86 %	β^-	1118.7 (38 %), 121.82, 539.49, ...
	^{91}Kr	8.57 s	3.35 %	β^-	108.79 (43.5 %), 412.04, 630.14, ...
	^{92}Kr	1.84 s	1.67 %	β^-	142.31 (64 %), 316.8, 1218.6, ...
	^{93}Kr	1.29 s	0.489 %	β^-, β^-n	253.42 (41.2 %), 182.02, 323.89, ...
	^{94}Kr	0.2 s	0.087 %	β^-, β^-n	219.47 (67.4 %), 186.32, 288.18, ...
	^{95}Kr	0.78 s	0.0072 %	β^-	-
	^{96}Kr	0.29 s	0.038 %	β^-	-
	^{97}Kr	0.1 s	2.97×10^{-5} %	β^-, β^-n	-
Xenon isotopes	^{129}Xe	Stable		-	-
	^{131m}Xe	11.9 d	0.034 %	I.T	163.97 (1.7 %)
	^{131}Xe	Stable	2.89 %	-	-
	^{132}Xe	Stable	4.31 %	-	-
	^{133m}Xe	2.19 d	0.192 %	I.T	233.5 (9.9 %)
	^{133}Xe	5.24 d	6.7 %	β^-	80.99 (36.6 %), 160.61, 302.85, ...
	^{134m}Xe	0.29 s	0.032 %	I.T	847.025 (100 %), 234.3, 884.09
	^{134}Xe	Stable	7.6 %	-	-
	^{135m}Xe	15.36 min	1.1 %	β^-, I.T	526.8 (81 %), 786.84, 1133, ...
	^{135}Xe	9.1 h	6.54 %	β^-	249.65 (89.8 %), 408, 608.6, ...
	^{136}Xe	Stable	0.4 %	-	-
	^{137}Xe	3.82 min	6.13 %	β^-	455.51 (31 %), 849, 1784, ...
	^{138}Xe	14.13 min	6.3 %	β^-	258.41 (31.5 %), 434.56, 1768.26
	^{139}Xe	39.68 s	5.04 %	β^-	218.75 (56 %), 296.7, 174.9, ...
	^{140}Xe	13.6 s	3.65 %	β^-	805.52 (20.5 %), 1413.66, 1315.05, ...
	^{141}Xe	1.73 s	1.25 %	β^-, β^-n	118.71 (16.1 %), 105.94, 540.12, ...
	^{142}Xe	1.22 s	0.439 %	β^-, β^-n	571.83 (1000 %), 618.31, 657.05, ...
	^{143}Xe	0.3 s	0.053 %	β^-	90 (0 %)
	^{144}Xe	1.15 s	0.006 %	β^-	-
	^{145}Xe	0.9 s	7.16×10^{-5} %	β^-, β^-n	-
	^{146}Xe	0.56 s	1.06×10^{-5} %	β^-	-

^{132}I ($T_{1/2}$ = 2.28 h). Iodine-132 remains among the other fission products for longer time than the other short-lived iodine isotopes mentioned above, since it is continuously regenerated from its parent ^{132}Te ($T_{1/2}$ = 3.26 d). Iodine-131 decays to ^{131m}Xe ($T_{1/2}$ = 11.9 d) which in turn decays to stable ^{131}Xe, whereas ^{132}I decays to stable ^{132}Xe. As mentioned above in Section 3.2.2, ^{131m}Xe did not appear in the gamma spectra of this work because of its low fission yield and low-abundance gamma rays. Figure 3.5 (a and b) shows the decay chains of ^{131}I, and ^{132}I as ^{235}U-fission products, whereas Table 3.2 compiles the nuclear characteristics and fission yields of ^{235}U-fission iodine isotopes.

The radioisotope ^{131}I is produced on a large scale in a special remotely-controlled apparatus either from fission of ^{235}U or from tellurium or tellurium oxide targets according to the nuclear reaction:

$$^{130}Te(n,\gamma)^{131}Te \xrightarrow[25\ min]{\beta^-} {}^{131}I$$

Quantity of ^{131}I produced by the latter reaction is limited by the thermal neutron cross-section (σ = 0.22 b) **(Şandru and Topa, 1968)** and abundance of ^{130}Te in the target as well as by neutron flux distribution in the irradiation facility **(Soenarjo et al., 1999)**. Whereas, an extremely high specific activity quantity of ^{131}I can be provided via $^{235}U(n,f)$ reaction with a fission yield of 2.89 %. Iodine-131 emits high-energy gamma rays (82.4 % of 364.49 keV) and particulate emissions. Beta particles with average energy = 192 keV, max energy = 607 keV are emitted and deposit the majority of their energy within 2.2 mm of their site of origin. ^{131}I has important applications in nuclear medicine in both diagnostic and therapeutic fields **(Maxon and Smith, 1990; Nordyke and Gilbert, 1991)**. ^{131}I is used for (i) diagnosis of the thyroid carcinoma, (ii) .the whole-body

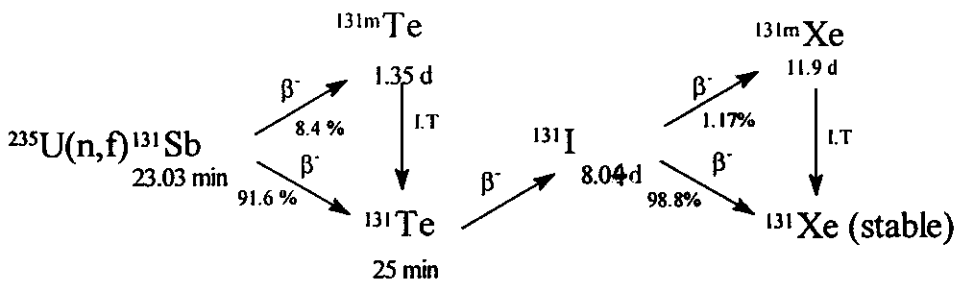

(a)

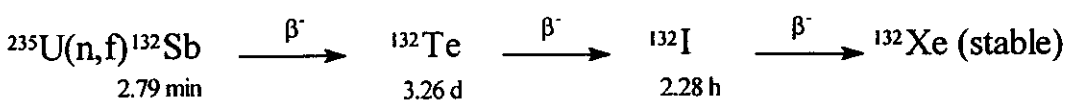

(b)

Figure 3.5. Decay chains of (a) ^{131}I and (b) ^{132}I as ^{235}U-fission products.

Table 3.2. Nuclear characteristics and fission yields of the ^{235}U-fission iodine isotopes.

Isotope	Half-life, $T_{1/2}$	Fission yield, Y_f	Decay mode	Main γ-energy (abundance), and other γ-energies in keV
^{127}I	Stable	0.156 %	-	-
^{129}I	1.57×10^7 y	0.511 %	β^-	29.78 (37 %), 29.46, 33.57, ...
^{131}I	8.04 d	2.89 %	β^-	364.49 (82.4%), 80.16, 284.31, 325.8, 636.9, 722.91, ...
^{132}I	2.28 h	4.31 %	β^-	667.68 (98.7%), 522.94, 630.21, 772.6, 812.2, 954.55, 1298, ...
^{133}I	20.8 h	6.7 %	β^-	529.5 (87.3 %), 875.3, 1298.9, ...
^{134}I	52.6 min	7.83 %	β^-	847.03 (95.4 %), 172.55, 884.09, ...
^{135}I	6.57 h	6.28 %	β^-	1260.41 (29 %), 1131.51, 1457.56, ...
^{136}I	1.39 min	2.64 %	β^-	1313.2 (67 %), 1321.2, 2289.6, ...
^{137}I	24.5 s	3.07 %	β^-	1218 (12.8 %), 600.5, 773.2, ...
^{138}I	6.49 s	1.49 %	β^-, β^-n	588.8 (56 %), 431, 483.7, ...
^{139}I	2.28 s	0.778 %	β^-, β^-n	527.7 (100 %), 571.2, 536.6 ...

iodine scans for following a patient with thyroid carcinoma, (iii) localization of tumors for removal, (iv) localization of the osteomyelitis infections, and (v) single-photon emission computed tomography (SPECT) imaging. ^{131}I therapy is used in treatment of (i) carcinoma of the thyroid (ii) the lymphoid tissue tumor/hyperthyroidism, (iii) the graves disease, (iv) the goiters, (v) the prostate cancer, (vi) the hepatocellular carcinoma, (vii) the melanoma, and (viii) treatment of spinal tumor.

3.3.1. Separation technique:

The alkali supernatant solution of fission products, containing iodine in the NaI form was transferred to the still (round-bottom flask) of the radioiodine-recovery system (Figure 2.2). Upon acidifying the solution by adding H_2SO_4, along with H_2O_2, iodide ion liberates as molecular I_2 according to:

$$H_2O_2 + 2NaI + H_2SO_4 \longrightarrow I_2 + Na_2SO_4 + 2H_2O$$

On adding H_2SO_4 acid to pH $\leq$ 10, aluminum content precipitates as $Al(OH)_3$ according to the following equation:

$$4NaAlO_2 + 2H_2SO_4 + 4H_2O \longrightarrow 4Al(OH)_3\downarrow + 2Na_2SO_4$$

With further addition of sulfuric acid to pH $\leq$ 5, aluminum hydroxide precipitate dissolves as follows:

$$4Al(OH)_3 + 6H_2SO_4 \longrightarrow 2Al_2(SO_4)_3 + 12H_2O$$

Adding up these two equations gives the net equation showing the conversion of the AlO_2^- to the Al^{3+} cation **((Agasyan, 1980)**, which is:

$$4NaAlO_2 + 8H_2SO_4 \longrightarrow 2Na_2SO_4 + 2Al_2(SO_4)_3 + 8H_2O$$

It is known that molecular iodine sublimes at room temperature. The acidified fission-products solution had to be boiled to increase the rate of iodine volatilization. Figure 3.6 (a, b, c, and d) shows the gamma spectra of the fission-products solution before and after acidification and boiling for different time periods. A current of air was introduced to the still of the radioiodine-recovery system and withdrawn by a pump, carrying the volatilized iodine. The air current passed through a water-cooled condenser to condense vapors of the sulfuric acid and collect them in a separate conical flask. Then, the air current passed through two successive acid traps (containing 15 and 5 ml of 3 M H_2SO_4, respectively) to retain any acid-soluble impurities might be distilled off along with molecular iodine and, also, to trap any species of iodine with oxidation numbers rather than zero, e.g., IO_3^- and/or I_2O_5. To recover the maximum possible amount of the radioiodine, the air current (after emerging from the second acid trap) passed through two successive alkali receivers (containing 15 and 5 ml of 0.1 M NaOH-0.01% $Na_2S_2O_3$ solution, respectively). The second alkali receiver was introduced to recover any amount of molecular iodine which might escape from the first one. For safety reasons, after its emergence from the second alkali receiver, the air current passed through a nitrogen-cooled filter containing charcoal impregnated with silver nitrate solution to retain any traces of the iodine that might escape from the second alkali receiver. Finally, the air current passed through the pump to ventilation.

Iodine was recovered in the alkali solution containing $Na_2S_2O_3$ in the NaI form as indicated by the following equation **(Agasyan, 1980)**:

$$I_2 + 2Na_2S_2O_3 \longrightarrow Na_2S_4O_6 + 2NaI$$

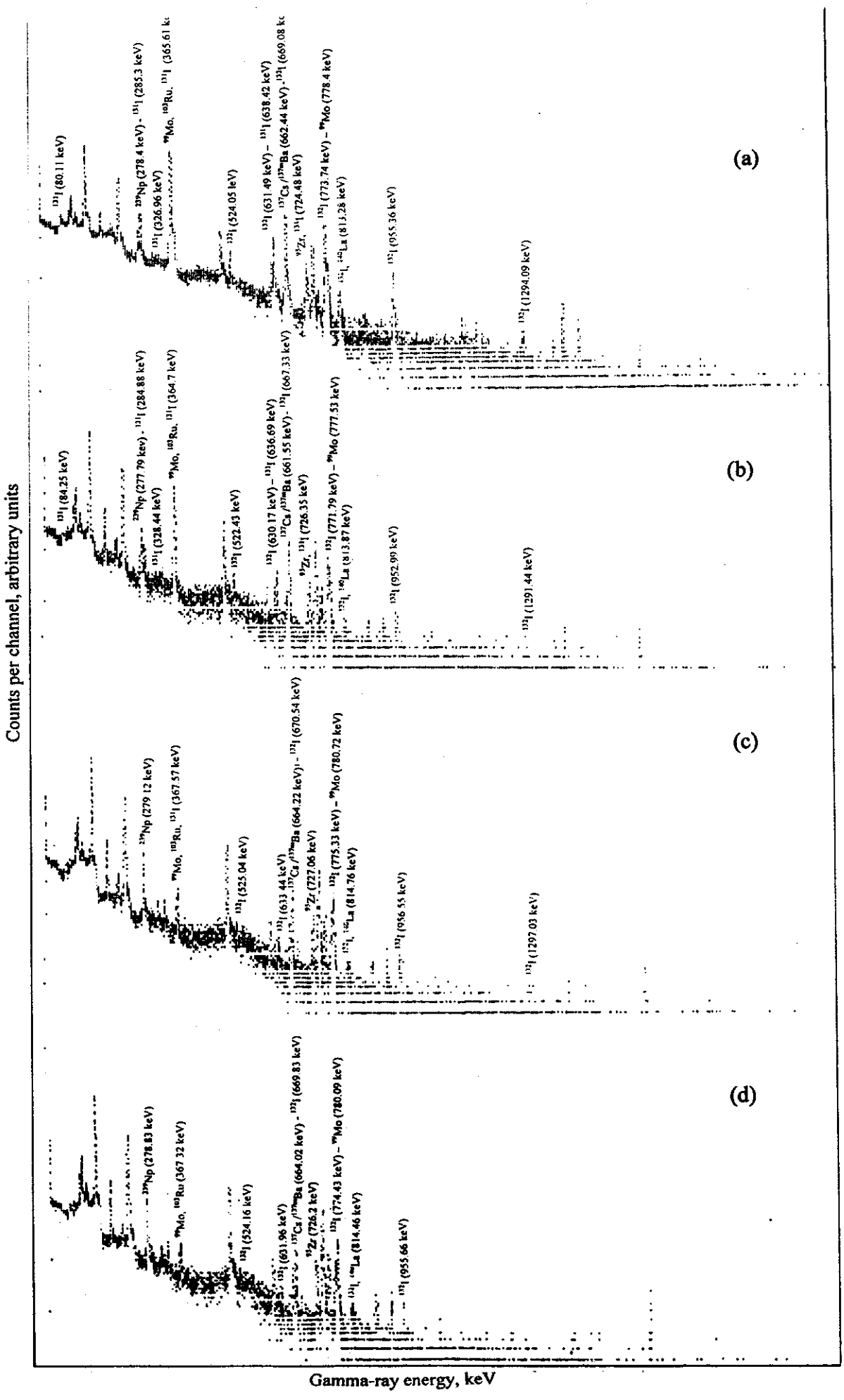

Figure 3.6. Gamma spectra of the fission-products solution (a) before acidification, and after acidification and boiling for (b) 2 h, (c) 3h, and (d) 3.5 h for separation of ^{131}I.

3.3.2. Quality control of the ^{131}I product:

3.3.2.1. Separation and recovery yields:

Figure 3.7 (a, b, c, and d) shows gamma spectra of the acid traps and the alkali receivers of the radioiodine-recovery system after boiling the acidified fission-products solution for 3.5 h. The only radioisotope detected in the acid traps and in the alkali receivers with ^{131}I was ^{132}I.

Table 3.3 compiles the radiometric analysis data of the isotopes ^{131}I and ^{132}I in: (i) the fission-products solution before acidification and after different times of boiling, and (ii) the acid traps and alkali receivers of the radioiodine-recovery system after boiling for 3.5 h. It should be mentioned that, there was an interference between the main γ-photopeak of ^{131}I (364.49 keV) and the two γ-photopeaks of ^{99}Mo and ^{103}Ru; 366.42 and 363.5 keV, respectively. As a result of this interference, these three peaks were appeared as one peak in the spectrum of the fission-products solution. Thus during boiling, the area under this peak decreased continuously as more ^{131}I was distilled off. After volatilization of all ^{131}I, the area under this peak became constant with further boiling. Boiling of the acidified fission-products solution (15 ml containing 20 % H_2SO_4 and 0.5 ml of 30 % H_2O_2) for 3.5 h was sufficient to remove more than 99.99 % of ^{131}I, i.e., the separation yield of ^{131}I ($S_{(I\text{-}131)}$) was > 99.99 %, where the area under the interference photopeak became constant with further boiling after 3.5 h.

According to data given in Table 3.3, total yield of recovered ^{131}I ($R_{(I\text{-}131)tot}$), defined by Equation 2.2, was found to be 97.31 %. Yield of ^{131}I recovered in the two acid traps ($R_{(I\text{-}131)acid}$), defined by Equation 2.3, was 23.71 % (22.16 % in the first one and 1.55 % in the second one), whereas that of ^{131}I recovered in the two alkali receivers, i.e., production yield of ^{131}I ($R_{(I\text{-}131)alk}$), defined by Equation 2.4, was 73.6 % (67.98 % in the first one and 5.62 % in the second one). Concerning ^{132}I, it was renewally generated in the fission-products solution from the decay of its parent ^{132}Te.

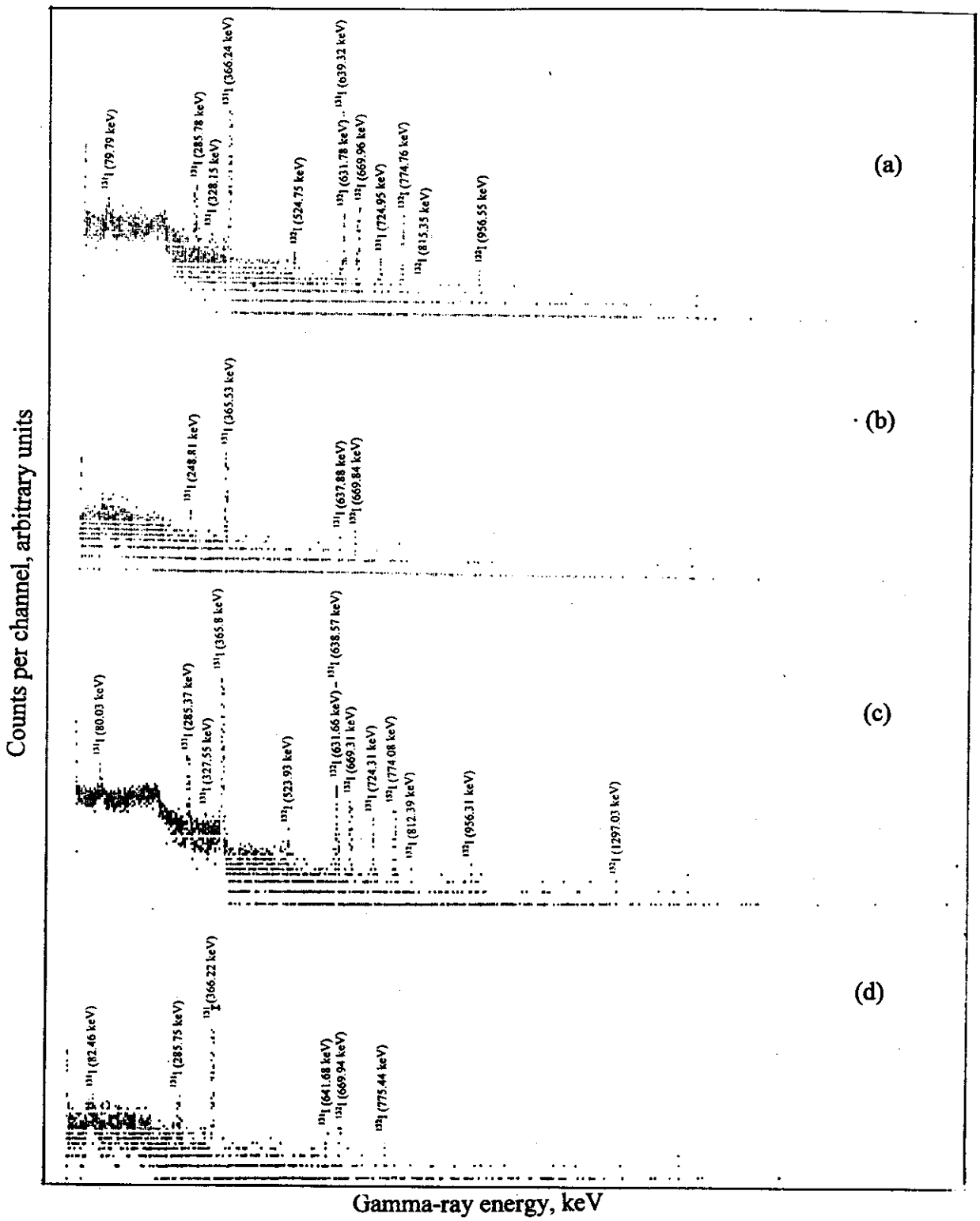

Figure 3.7. Gamma spectra of (a) the first acid trap (b) the second acid trap, (c) the first alkali receiver, and (d) the second alkali receiver of the radioiodine-recovery system.

Table 3.3. Radiometric analysis data for separation and recovery of ^{131}I.

Isotope			^{131}I	^{132}I
Centroids (CTRDs) of the obtained γ-photopeaks in keV	Fission-products (F.P) solution	Before boiling	365.61, 80.11, 285.3, 326.96,638.42, 724.48	669.08, 524.05,631.49, 773.74, 813.28, 955.36, 1294.09
		After boiling for 2 h	364.7, 84.25, 284.88, 328.44, 636.69, 726.35	667.33, 522.43, 630.17, 771.79,813.87,952.99, 1291.44
		After boiling for 3 h	367.57	670.54, 525.04, 633.44, 775.33, 814.76, 956.55, 1297.03
		After boiling for 3.5 h	Not detected	669.83, 524.16, 631.96, 774.43, 814.46, 955.66
	Acid traps	First one	366.24, 79.79, 285.78, 328.15, 639.32, 724.95	669.96, 524.75, 631.78, 774.76, 815.35, 956.55
		Second one	365.53, 248.81, 637.88	669.84
	Alkali receivers	First one	365.8, 80.03, 285.37, 327.55, 638.57, 724.31	669.31, 523.93, 631.66, 774.08, 812.39, 956.31, 1297.03
		Second one	366.22, 82.46, 285.75, 641.68	669.94, 775.44
	Charcoal filter		Not detected	Not detected
Net area under the main γ-photopeak (normalized to the total volume of the solution)	F.P Solution	Before boiling	9489600	863880
		After boiling for 2 h	1358700	158100
		After boiling for 3 h	56970	40635
		After boiling for 3.5 h	-	21000
	Acid traps	First one	2102886	36705
		Second one	147090	2455
	Alkali receivers	First one	6450935	103860
		Second one	533240	8340
	Charcoal filter		-	-

In most cases, no detectable amounts of radioiodine were found in the charcoal filter at end of the distillation process.

The fraction of the volatilized ^{131}I, < 2.68 %, which was not recovered in the acid traps or in the alkali receivers might be condensed during passage of the air current through the water-cooled condenser. A part of it deposited on the glass walls of the condenser and the other part was collected along with the condensed vapors of the sulfuric acid in the conical flask attached to the condenser.

The fraction of ^{131}I found in the acid traps may support the suggestion that ionic species of iodine might be formed and distilled off during distillation of I_2 (Section 3.3.1). For example, HIO_3 gives monomeric IO_2HSO_4 in a dilute solution of sulfuric acid. Also, the so-called iodosyl sulfate $(IO)_2SO_4$, which is a yellow solid, obtained by the action of H_2SO_4 on I_2O_5. $(IO)_2SO_4$ has polymeric $(I\text{-}O)_n$ chains cross-linked by the anion **(Cotton and Wilkinson, 1979)**.

3.3.2.2. Radionuclidic purity:

The first alkali receiver was chosen to calculate radionuclidic purity of the recovered ^{131}I, because of its higher radioactivity. Radionuclidic purity of ^{131}I is defined as "fraction of γ-radioactivity of the first alkali receiver contributed to ^{131}I to the total γ-radioactivity". According to radiometric analysis data mentioned in Table 3.3, the radionuclidic purity of ^{131}I recovered in the first alkali trap was found to be 98.28 % measured immediately at end of the distillation process. Radiometric analysis data showed that 1.72 % of the total γ-radioactivity of the first alkali receiver was due to ^{132}I. No further radionuclides were identified in the acid traps or in the alkali receivers.

Radionuclides of the first alkali receiver (^{131}I and ^{132}I) were further identified by their characteristic half-lives obtained from their decay curves

as indicated in Figures 3.8 and 3.9. Figure 3.8 (a and b) shows the gross-gamma radioactive decay curves of the first alkali trap of the radioiodine-recovery system followed for 24 h and 190 h, while Figure 3.9 (a and b) shows the individually analyzed decay curves of ^{131}I and ^{132}I. After 140 d, no residual radioactivity was detected in the first alkali receivers. Slopes of the decay curves of ^{131}I and ^{132}I (Figure 3.9, a and b) were corresponding to half-lives of 8.4 d and 2.3 h, respectively.

3.3.2.3. Radiochemical purity:

The first alkali receiver was chosen to calculate the radiochemical purity of the radioiodine product, because it received majority of the radioiodine. Radiochemical purity of the iodine product is defined as "ratio of the iodine γ-radioactivity found in the desired chemical form, i.e., I^-, to the total γ-radioactivity of iodine". By using a strip of "Whatman No. 1" paper (25 cm long and 1.5 cm wide) as a stationary phase and a mixture of 70 % methanol and 30 % H_2O as the developing mobile phase in an ascending paper chromatography technique, one R_f value (Equation 2.8) of ~ 0.73 was obtained in agreement with the published R_f value (0.7) which may refer to the presence of I^- and/or I^{3-} ions **(Baldwin, 1986)**. To be sure that the R_f value of ~ 0.73 obtained with "Whatman No.1" paper referred only to I^- and not to I^{3-}, the same procedure was carried out using a strip of TLC with silica gel (also 25 cm long and 1.5 cm wide) and a solvent consisted of a mixture of isopropyl alcohol, ethyl acetate, 6 M ammonium hydroxide, and acetone (35:30:25:20 by volume, respectively). In this case, R_f value of ~ 0.8 was obtained in agreement with the published R_f value (0.82) which refers only to the presence of I^- ion **(Baldwin, 1986).**

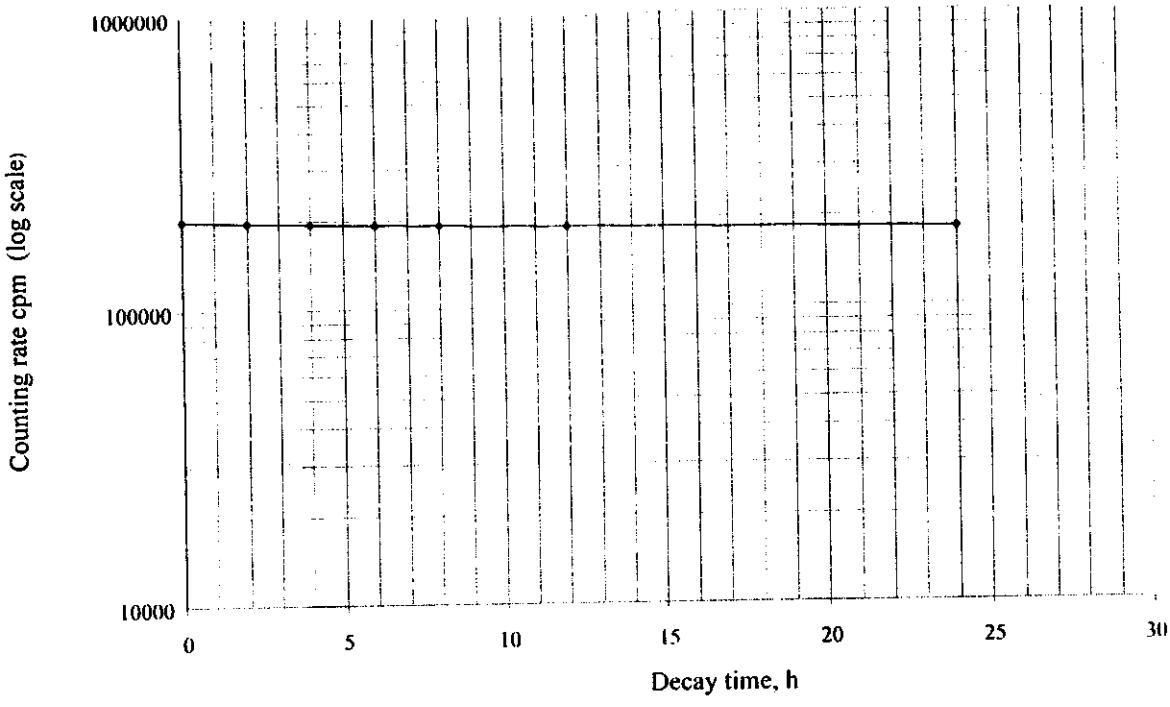

(a)

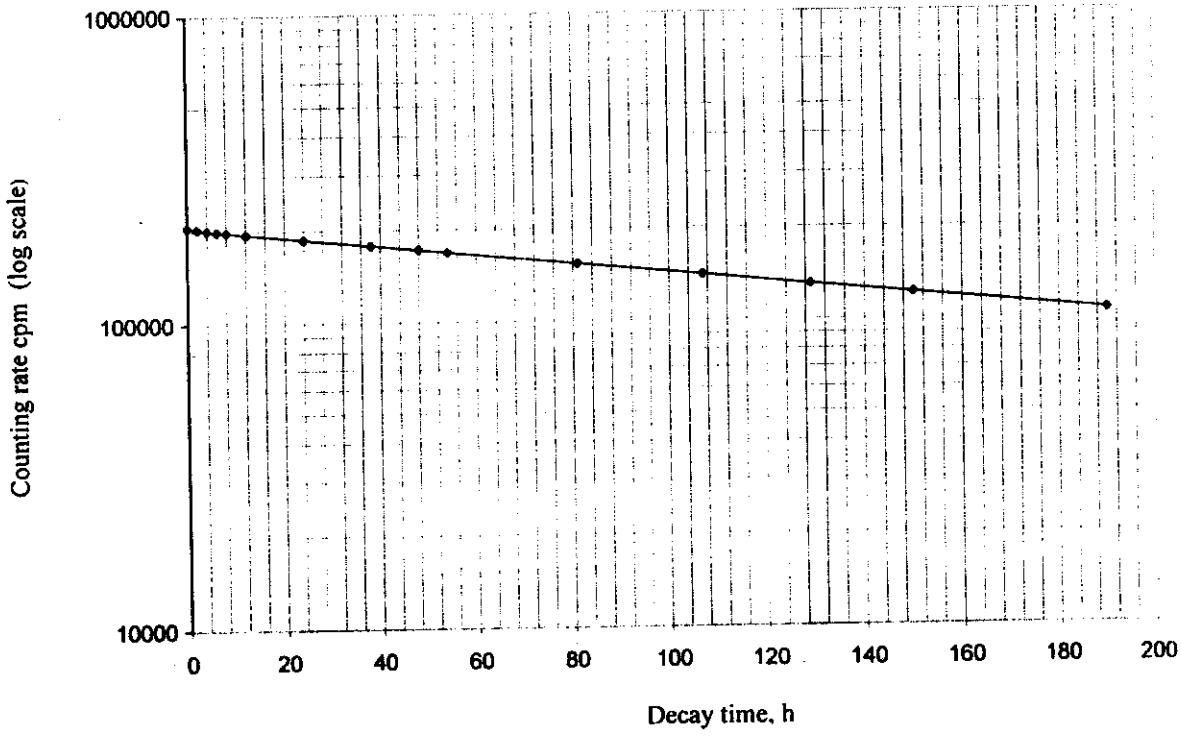

(b)

Figure 3.8. Gross-gamma radioactive decay curves of the first alkali receiver of the radioiodine-recovery system followed for (a) 24 h and (b)190 h.

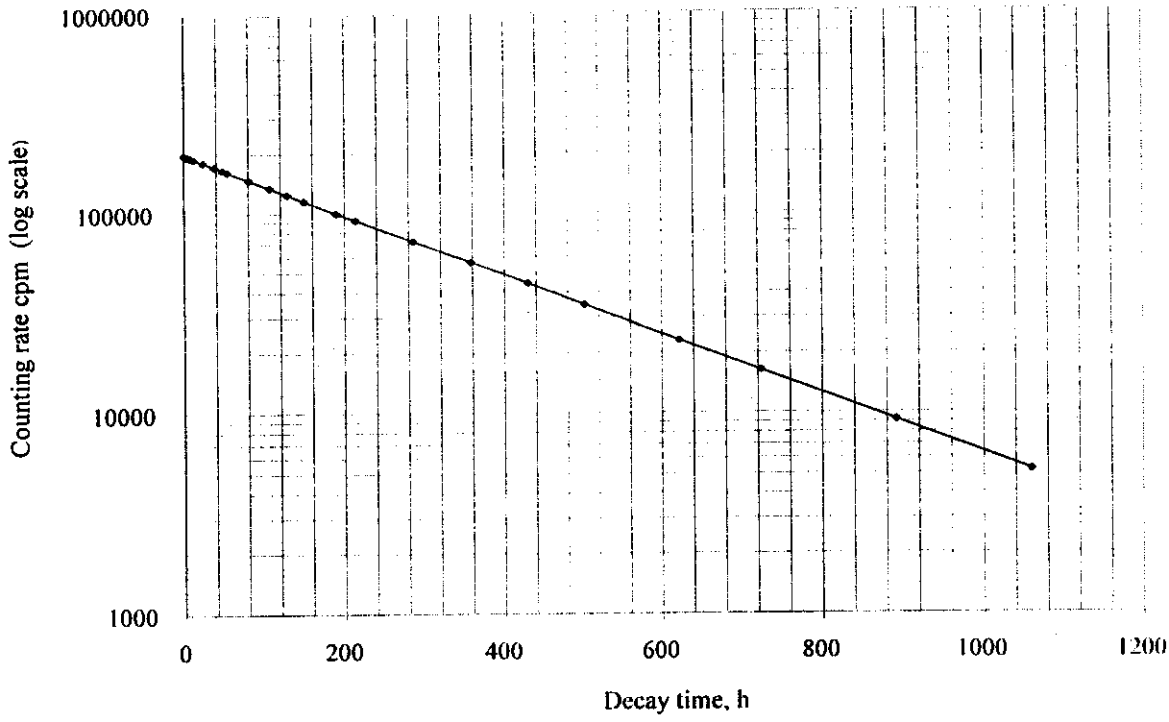

(a)

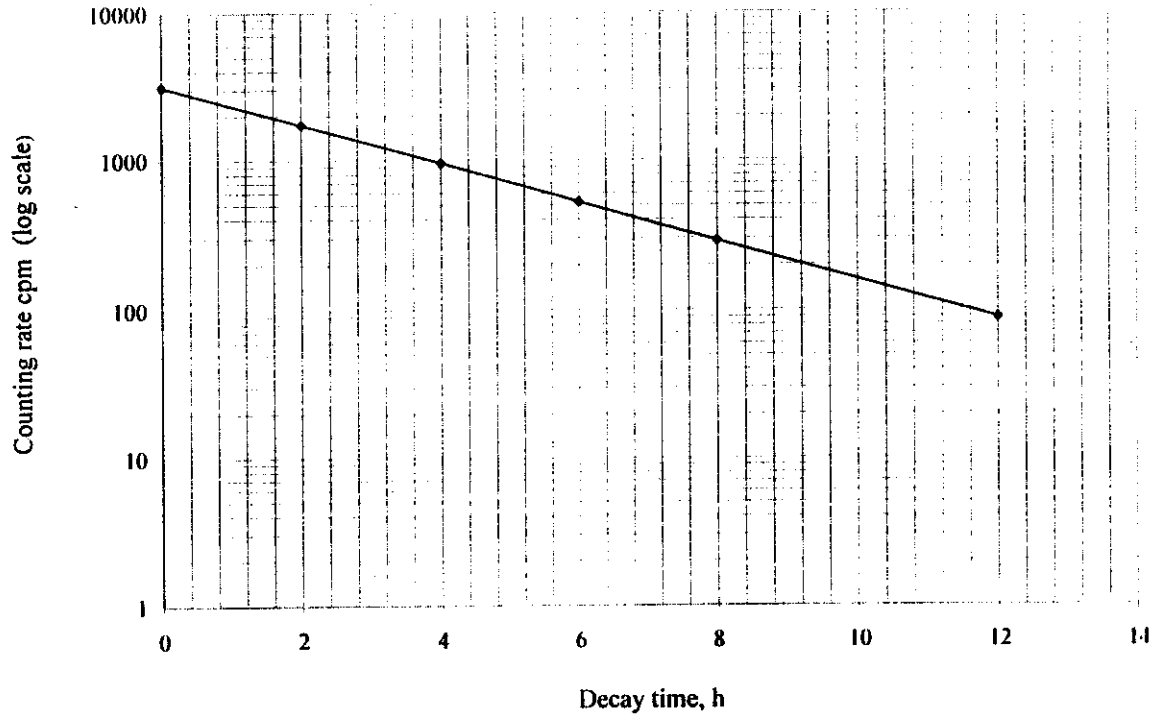

(b)

Figure 3.9. Individual decay curves of (a) ^{131}I and (b) ^{132}I recovered in the first alkali receiver of the radioiodine-recovery system.

Figure 3.10 (a and b) shows the radiochromatograms of the ^{131}I product obtained by using "Whatman No.1" paper and by using the TLC (with silica gel). With "Whatman No.1" paper, radiochemical purity (as I^-) was found to be 99.81 %, while it was 99.76 % with TLC.

3.3.2.4. pH-value of the product solution:

At end of the radioiodine distillation process, pH-value of both of the first and second alkali receivers was found to be 12.8; this value is suitable to avoid formation of volatile elemental iodine.

3.3.2.5. Radioactivity and specific activity:

Radioactivity of the recovered ^{131}I, $A_{(I\text{-}131)}$, was calculated according to:

$$A_{(I\text{-}131)} = R_{(I\text{-}131)alk} \left(A_{0(I\text{-}131)} e^{-\lambda_{(I\text{-}131)} t} \right) \qquad (3.1)$$

Where,

$A_{0(I\text{-}131)}$ = radioactivity of ^{131}I obtained at end of irradiation, it was calculated by using Equation (1.3).

t = elapsed time period between end of the target irradiation and completion of the radioiodine separation (8 d).

For weights of 0.02, 0.06, and 0.1 g of the irradiated UO_3 targets, calculated values of $A_{(I\text{-}131)}$ were found to be < 898, < 2694, and < 4490 μCi, respectively. Radioactivity of the recovered ^{131}I was, of course, lower than the calculated value because there was a fraction of the fission-iodine escaped during the irradiation, cooling, and digestion processes.

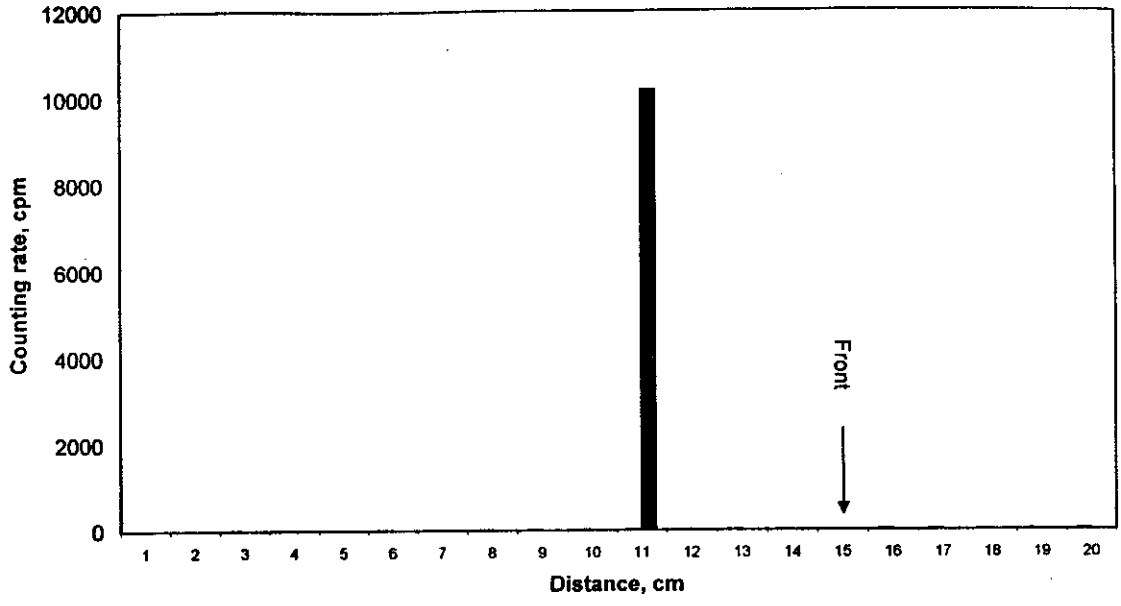

(a)

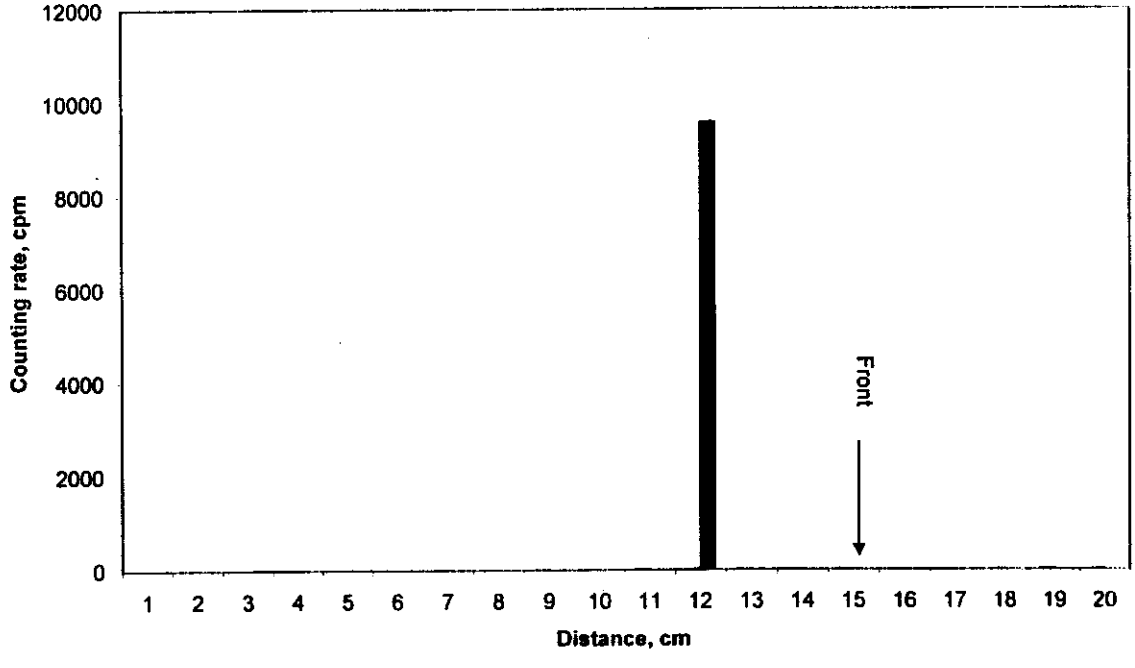

(b)

Figure 3.10. Radiochromatograms of the ^{131}I product obtained by using (a) "Whatman No.1" paper and (b) TLC (with silica gel).

Specific activity of the produced ^{131}I (μCi/ml) could be calculated by dividing $A_{(I-131)}$ by total volume of the two alkali receivers (20 ml), after mixing them. For weights of 0.02, 0.06, and 0.1 g of the irradiated UO_3 targets, calculated specific activities of the recovered ^{131}I were found to be < 45, < 135, and < 225 μCi/ml, respectively. Alternatively, the two alkali receivers of the radioiodine-recovery system might not be mixed to keep the higher specific-activity of ^{131}I in the first alkali receiver. Table 3.4 compiles the quality control data of the ^{131}I product.

3.3.3. Precautions of separation, handling, and storage of radioiodine:

Volatility of the elemental iodine, as molecular I_2, is the most significant problem accompanying this element. When the radioiodine is to be separated (from the other fission products), handled, or stored, the following precautions must be taken into consideration:

1. Before its use, the radioiodine-recovery system must be tested to ensure that there is no leakage in pass of the radioiodine; this is to avoid the internal contamination with radioiodine via smelling.
2. Solutions containing radioiodide ions should neither be made acidic, nor stored frozen; both lead to formation of the volatile elemental iodine **(Liverpool University, 2001)**. When possible, solutions containing radioiodide ions should be kept having pH above 8.
3. Simply opening a vial of $Na^{131}I$ at a high radioactive concentration can cause minute droplets to become airborne. Vials containing radioiodine should be opened in the fume hood.
4. Double gloves should be worn during handling of radioiodine, as iodine has been shown to penetrate one thickness of plastic gloves **(Suny Upstate Medical University, 2001)**.

Table 3.4. Quality control data of the ^{131}I product.

Separation yield, $S_{(I-131)}$		> 99.99 %
Production yield, $R_{(I-131)alk}$		73.6 %
Radionuclidic purity		98.28 %
% Other radionuclides		1.72 % ^{132}I
Radiochemical purity (as iodide), %	By using "Whatman No.1" paper	99.81 %
	By using TLC (with silica gel)	99.76 %
pH-value		12.8
Calculated radioactivity, µCi	0.02 g of UO_3	< 898
	0.06 g of Uo_3	< 2694
	0.1 g of UO_3	< 4490
Calculated specific activity, µCi/ml	0.02 g of UO_3	< 45
	0.06 g of UO_3	< 135
	0.1 g of UO_3	< 225

3.4. Production of radioruthenium:

Figure 3.1 (b) indicates presence of the γ-photopeaks of ^{103}Ru (499.42 and 366.33 keV). Fission reactions of ^{235}U give rise to seven ruthenium isotopes; ^{99}Ru, ^{101}Ru, ^{102}Ru, ^{103}Ru, ^{104}Ru, ^{105}Ru, and ^{106}Ru. The isotopes of ^{99}Ru, ^{101}Ru, ^{102}Ru, and ^{104}Ru are stable ones, whereas ^{105}Ru ($T_{1/2}$ = 4.44 h) decayed practically, completely during the seven-days cooling period. Ruthenium-103 ($T_{1/2}$ = 39.27 d) and ruthenium-106 ($T_{1/2}$ = 1.02 y) are the most important fission-ruthenium isotopes. More than 95 % of ^{103}Ru decays to ^{103m}Rh ($T_{1/2}$ = 56.12 min) which in turn decays to the stable ^{103}Rh. Remaining of ^{103}Ru (<5 %) decays directly to ^{103}Rh. ^{103m}Rh did not appear in any of gamma spectra of this work because of its low-energy gamma rays (39.76 keV). ^{106}Ru is a pure β^--emitter and decays to ^{106}Rh ($T_{1/2}$ = 29.9 s) which in turn decays to stable ^{106}Pd. Figure 3.11 (a and b) shows decay chains of ^{103}Ru and ^{106}Rh as ^{235}U-fission products, while Table 3.5 compiles the nuclear characteristics and fission yields of the ruthenium and rhodium isotopes produced from fission reactions of ^{235}U.

Ruthenium is one of the most troublesome elements in nuclear chemical engineering, where it causes many problems during reprocessing of the spent nuclear fuel by the PUREX process and the following aqueous waste treatment because of its multiple valence states and complex chemistry **(Lee and Bang, 1983; Sato, 1982)**.

Ruthenium-103 is produced with a fission yield of 3.03 % and emits high-energy gamma rays (91.1 % of 497.04 keV). It has important applications in nuclear medicine in fields of myocardial blood flow, radiolabeling microspheres, and positron emission tomography (PET) imaging **(NMRC, 1998)**.

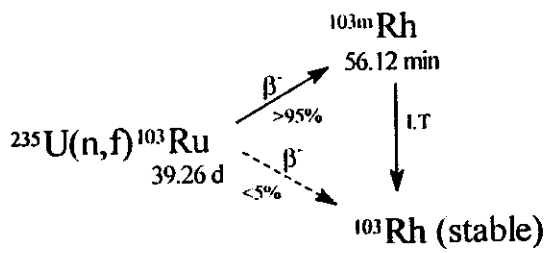

(a)

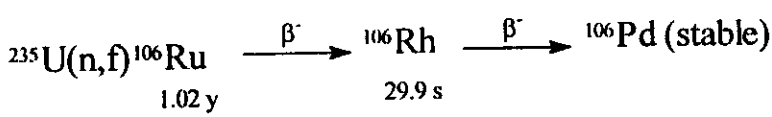

(b)

Figure 3.11. Decay chains of (a) ^{103}Ru and (b) ^{106}Rh as ^{235}U-fission products.

Table 3.5. Nuclear characteristics and fission yields of the ^{235}U-fission ruthenium and rhodium isotopes.

Isotope		Half-life, $T_{1/2}$	Fission yield, Y_f	Decay mode	Main γ-energy (abundance), and other γ-energies in keV
Ruthenium isotopes	^{99}Ru	Stable		-	-
	^{101}Ru	Stable	5.17 %	-	-
	^{102}Ru	Stable	4.3 %	-	-
	^{103}Ru	39.27 d	3.03 %	β^-	497.04 (91.1%), 363.5, 557, 610.33, ...
	^{104}Ru	Stable	1.88 %	-	-
	^{105}Ru	4.44 h	0.964 %	β^-	724.2 (49 %), 316.5, 469.38, 676.32, ...
	^{106}Ru	1.02 y	0.402 %	β^-	-
Rhodium isotopes	^{103m}Rh	56.12 min	3.03 %	I.T	39.76 (0.068 %)
	^{103}Rh	Stable	3.03 %	-	-
	^{105m}Rh	40 s	0.964 %	I.T	129.53 (20.2 %)
	^{105}Rh	35.36 h	0.964 %	β^-	319.24 (19.2 %), 306.31, 319.14, ...
	^{106}Rh	29.9 s	0.402 %	β^-	511.80 (20.5 %), 621.80, ...

3.4.1. Separation technique:

After separation of radioiodine, the still of the radioiodine-recovery system (containing the acidified fission-products solution) was connected to the radioruthenium-recovery system (Figure 2.2). Excess of sulfuric acid was added to the fission-products solution along with $KMnO_4$. Under these conditions, potassium permanganate is reduced according to:

$$MnO_4^- + 8H^+ + 5e^- = Mn^{2+} + 4H_2O$$

while ruthenium is oxidized to ruthenium tetroxide, RuO_4, **(Cotton and Wilkinson, 1979; Lee and Bang, 1983)**. RuO_4 is a volatile yellow compound (m.p. 25.5°C) **(Lide, 1992-1993)** which sublimes at room temperature. To promote volatilization of the formed RuO_4 from the fission-products solution, boiling was applied. Figure 3.12 (a and b) shows the gamma spectra of the fission-products solution (after separation of ^{131}I) before and after boiling of the acidified fission-products solution (40 % H_2SO_4) for 40 min. In a similar manner as shown for recovery of fission radioiodine, an air current was introduced to the still to carry the volatilized RuO_4. The air current passed through a water-cooled condenser and subsequently through two successive alkali receivers (containing 15 and 5 ml of 0.1 M NaOH solution, respectively). The second alkali receiver was introduced to recover any traces of the ruthenium tetroxide which might escape from the first receiver. After emerging from the second alkali receiver, the air current passed through a nitrogen-cooled charcoal filter to absorb any traces of radioruthenium that might escape from the second alkali receiver. Finally, the air current passed through the pump to the ventilation.

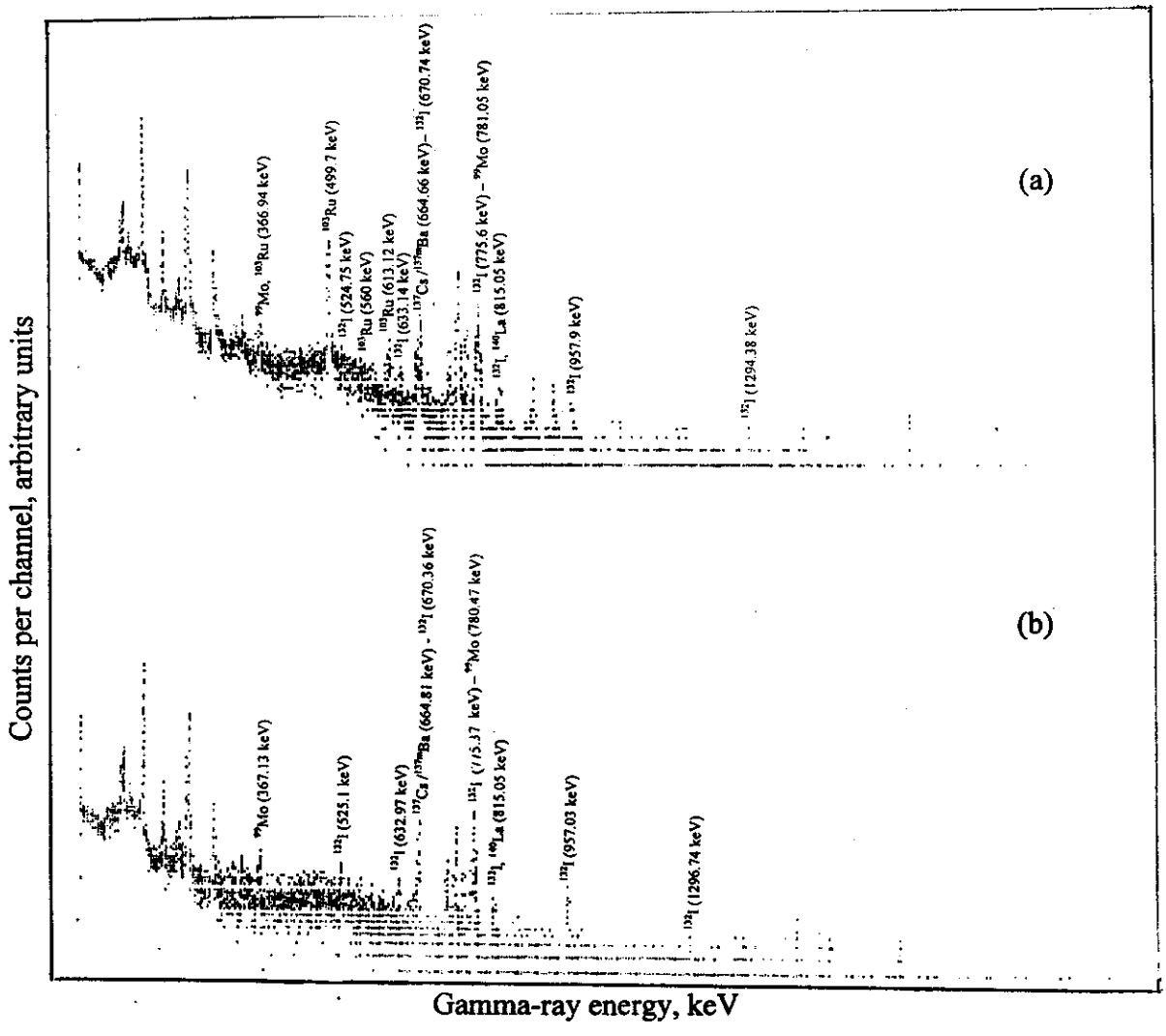

Figure 3.12. Gamma spectra of the fission-products solution (a) after separation of ^{131}I and (b) after raising concentration of H_2SO_4 to 40 % and boiling for 40 min.

In the NaOH solution, ruthenium tetroxide is dissolved and reduced to form perruthenate, RuO_4^-, which is then reduced again to form ruthenate according to the following two equations **(Cotton and Wilkinson, 1979)**:

$$4RuO_4 + 4OH^- \longrightarrow \underset{\text{perruthenate}}{4RuO_4^-} + 2H_2O + O_2$$

$$4RuO_4^- + 4OH^- \longrightarrow \underset{\text{ruthenate}}{4RuO_4^{2-}} + 2H_2O + O_2$$

3.4.2. Quality control of the ^{103}Ru product:

3.4.2.1. Separation and recovery yields:

Figure 3.13 shows the gamma spectrum of the alkali receiver of the radioruthenium-recovery system after boiling the acidified fission-products solution for 40 min. As shown in Figure 3.13, three isotopes were appeared in the gamma spectrum of the first alkali receiver; these were ^{103}Ru, ^{106}Rh and ^{132}I.

Table 3.6 compiles the radiometric analysis data of the isotopes ^{103}Ru, ^{106}Rh, and ^{132}I in (i) the fission-products solution before distillation of the ruthenium tetroxide and after boiling for 40 min, and (ii) the first alkali receiver of the radioruthenium-recovery system after boiling for 40 min. It was found that boiling of the acidified fission-products solution (15 ml of 40 % sulfuric acid containing 0.01 g of $KMnO_4$) for 40 min was quite sufficient to remove more than 99.99 % of ^{103}Ru, i.e., separation yield of ^{103}Ru ($S_{(Ru\text{-}103)}$) was > 99.99 %. The recovery yield, i.e., production yield, of ^{103}Ru ($R_{(Ru\text{-}103)}$) defined by Equation 2.5 was found to be 65.03 % and totally collected in the first alkali receiver. No radioactivity was detected in both the second alkali receiver and the charcoal filter. The fraction of the distilled off ^{103}Ru which was not detected in the alkali receivers (< 34.96 %), might be deposited on walls of the condenser and could be

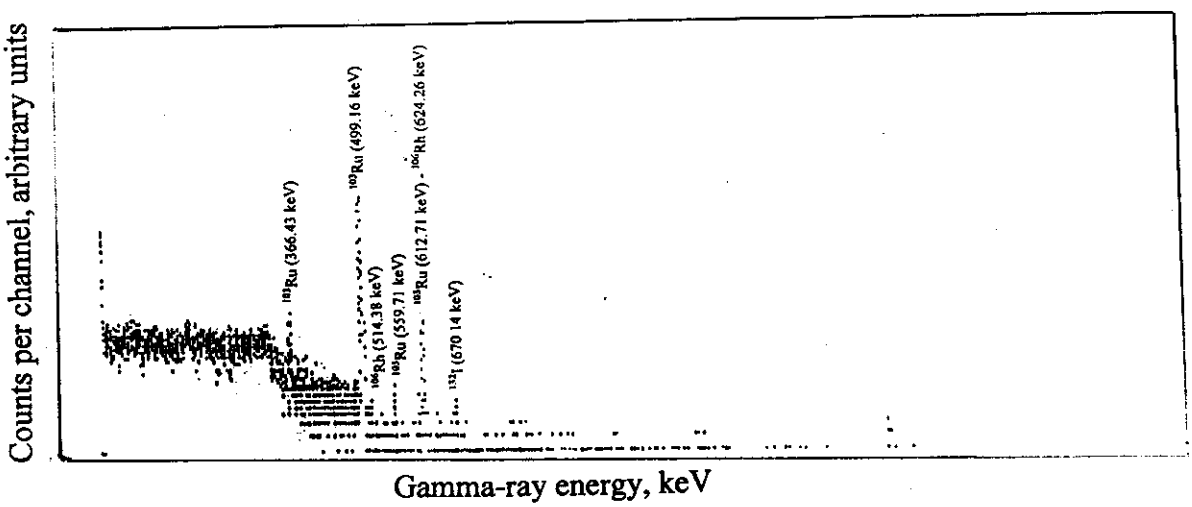

Figure 3.13. Gamma spectrum of the alkali receiver of the radioruthenium-recovery system.

Table 3.6. Radiometric analysis data for separation and recovery of ^{103}Ru.

Isotope			^{103}Ru	^{106}Rh	^{132}I
CTRDs of the obtained γ-photopeaks in keV	F.P solution	Before boiling	499.7, 366.94, 560, 613.12	Not detected	670.74, 524.75, 633.14, 775.6, 815.05, 957.9, 1294.38
		After boiling for 40 min	Not detected	Not detected	670.36, 525.1, 632.97, 775.37, 815.05, 957.03, 1296.74
	Alkali receivers	First one	499.16, 366.43, 559.71, 612.71	514.38, 624.26	670.14
		Second one	Not detected	Not detected	Not detected
	Charcoal filter		Not detected	Not detected	Not detected
Net area under the main γ-photopeak (normalized to the total volume of the solution)	F.P Solution	Before boiling	325740	-	34560
		After boiling for 40 min	-	-	23772
	Alkali receivers	First one	211825	11100	7865
		Second one	-	-	-
	Charcoal filter		-	-	-

easily recovered by washing the condenser with a few milliliters of 0.1 M NaOH solution.

3.4.2.2. Radionuclidic purity:

According to the data given in Table 3.6, Radionuclidic purity of the recovered ^{103}Ru, i.e., fraction of the total γ-radioactivity of the first alkali receiver contributed to ^{103}Ru, was found to be 91.78 % at end of the ruthenium tetroxide distillation process. Radionuclide contaminants of 4.81 % and 3.41 % of the total γ-radioactivity of the first alkali receiver were due to ^{106}Rh and ^{132}I, respectively.

Presence of ^{132}I along with ^{103}Ru in the first alkali receiver was due to volatilization of the former, which was continuously generated in the fission-products solution from the decay of its parent nuclide ^{132}Te. Contribution of the ^{132}I radioactivity to the total radioactivity of the alkali receiver of the radioruthenium recovery-system depends on the time left from end of the ^{131}I separation process to beginning of the ^{103}Ru separation process (considering the irradiation time, the neutron flux, and the cooling time are constant). The time at which the ^{132}I generated from ^{132}Te reaches its maximum radioactivity, T_{max}, is ~12 h and can be calculated as follows **(Choppin and Rydberg, 1980)**:

$$T_{max} = \frac{\ln (\lambda_1 / \lambda_2)}{\lambda_2 - \lambda_1} \qquad (3.2)$$

Where,

λ_1 = decay constant of ^{132}Te (8.86×10^{-3} h^{-1}).

λ_2 = decay constant of ^{132}I (0.30 h^{-1}).

3.4.2.3. pH-value of the product solution:

At end of the distillation process, pH-value of the first alkali receiver, of the radioruthenium-recovery system, was found to be 12.

3.4.2.4. Radioactivity and specific activity:

Radioactivity of the recovered ^{103}Ru, $A_{(Ru\text{-}103)}$, was calculated according to:

$$A_{(Ru\text{-}103)} = R_{(Ru\text{-}103)alk} \left(A_{0(Ru\text{-}103)} e^{-\lambda_{(Ru\text{-}103)} t} \right) \qquad (3.3)$$

Where,

$A_{0(Ru\text{-}103)}$ = radioactivity of ^{103}Ru obtained at end of irradiation, it was calculated by using Equation (1.3).

Separation of ^{103}Ru took less than one hour, so that t in Equation (3.3) was also considered to be 8 d. For weights of 0.02, 0.06, and 0.1 g of the irradiated UO_3 targets, calculated values of $A_{(Ru\text{-}103)}$ were found to be 293, 880, and 1466 μCi, respectively.

Specific activity of ^{103}Ru (μCi/ml) could be calculated by dividing $A_{(Ru\text{-}103)}$ by volume of the first alkali receiver solution (18 ml). Thus for weights of 0.02, 0.06, and 0.1 g of the irradiated UO_3 targets, calculated specific activities of the recovered ^{103}Ru were found to be 16, 49, and 81 μCi/ml, respectively. Table 3.7 shows the quality control data of the ^{103}Ru product.

3.4.3. Precautions of separation of radioruthenium:

In addition to risks of the internal contamination with its radioactivity by smelling, ruthenium tetroxide vapor is irritating to the eyes and respiratory tract. Because of these risks, pass of the RuO_4 vapor in the

Table 3.7. Quality control data of the ^{103}Ru product.

Separation yield, $S_{(Ru-103)}$		> 99.99 %
Recovery yield, $R_{(Ru-103)}$		65.03 %
Radionuclidic purity		91.78 %
% Other radionuclides		4.81 % ^{106}Rh and 3.41 % ^{132}I
pH value		12
Calculated radioactivity, µCi	0.02 g of UO_3	293
	0.06 g of UO_3	880
	0.1 g of UO_3	1466
Calculated specific activity, µCi/ml	0.02 g of UO_3	16
	0.06 g of UO_3	49
	0.1 g of UO_3	81

radioruthenium-recovery system should be tested against leakage before the use.

3.5. Batch separation of Sr, Ba, La, and Ce radionuclides:

3.5.1. Separation technique:

In the acidified fission-products solution, both of the strontium and barium isotopes formed acid-insoluble sulfates; $SrSO_4$ and $BaSO_4$, respectively **(Agasyan, 1980).** The concentrations of carrier-free strontium and barium, produced from ^{235}U-fission reactions, are very small and subsequently, the formed $SrSO_4$ and $BaSO_4$ were very small so that these sulfates were not precipitated (Figure 3.14, a). Thus, addition of inactive barium as a carrier to the acidified fission-products solution was necessary to carry down the formed fission-barium and -strontium sulfates. Barium chloride carrier was prepared by dissolving barium carbonate in hydrochloric acid according to:

$$BaCO_3 + 2HCl \longrightarrow BaCl_2 + H_2O + CO_2\uparrow$$

Before addition of $BaCl_2$ solution, the acidified fission-products solution was transferred from the still to a conical flask. On adding $BaCl_2$ (dropwise to attain homogeneity), the formed $BaSO_4$ precipitated, carrying with it the sulfates of fission barium and strontium, according to the following equation **(Agasyan, 1980)**:

$$BaCl_2 + H_2SO_4 \longrightarrow BaSO_4\downarrow + 2HCl$$

Since Ba^{2+} was added to an excess of SO_4^{2-}, the formed $BaSO_4$ precipitate was considered to be surrounded by SO_4^{2-} ions. These charge-like particles repelled each other and, subsequently, the precipitate particles

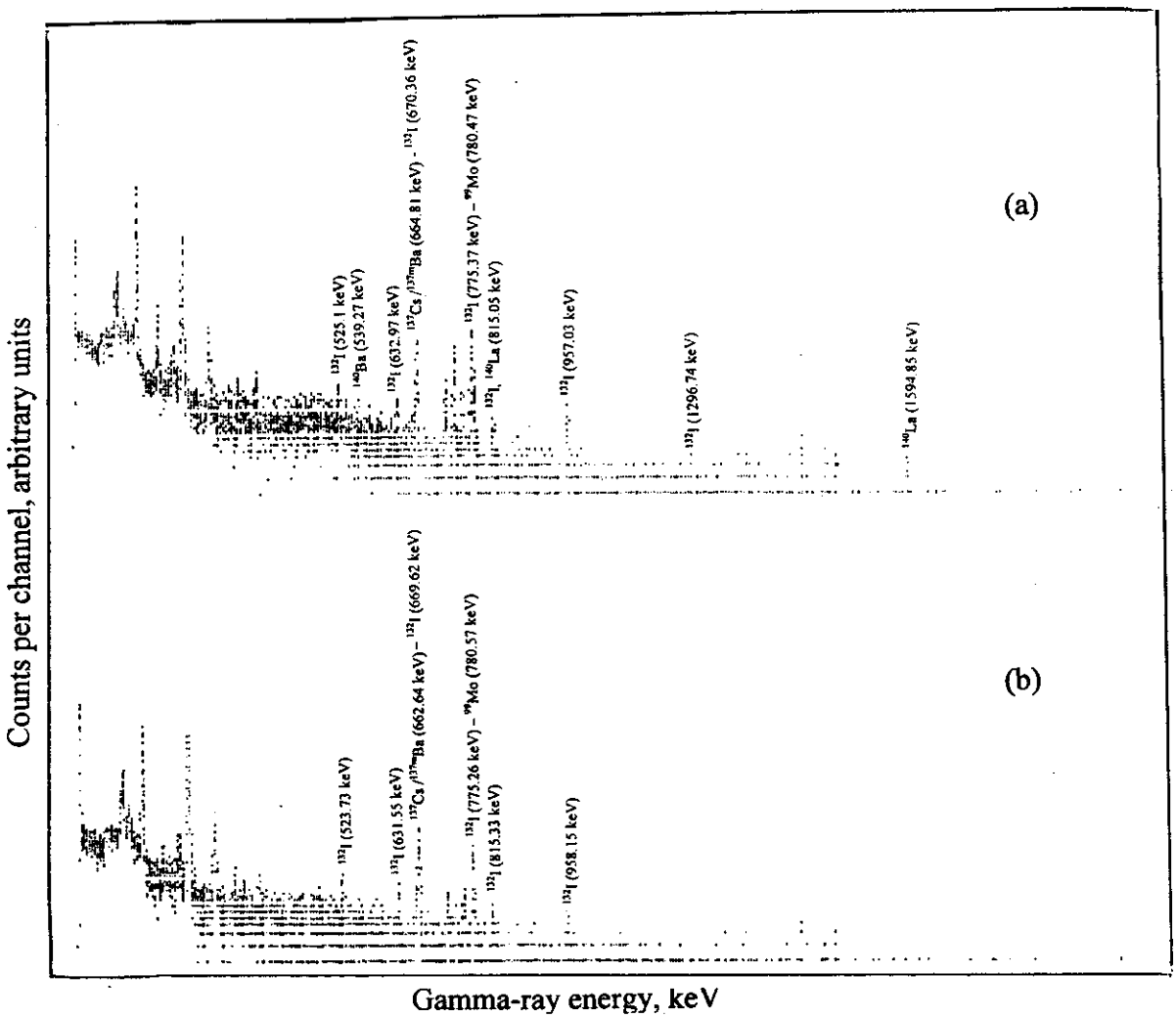

Figure 3.14. Gamma spectra of the fission-products solution (a) before addition of $BaCl_2$ and (b) after addition of $BaCl_2$ and separation of the formed precipitate.

were small and dispersed in the solution, so that they did not settle rapidly **(Seely, 2001)**. These negatively charged barium sulfate particles adsorbed some cations from the solution. Most of these cations were removed by washing of the formed precipitate as will be mentioned below. To obtain complete precipitation of the barium sulfate, the solution should be either heated (not boiled) for 1 h to enhance coagulation of the precipitated particles, or allowed to stand at the laboratory temperature for about 18 h **(Vogel, 1961)**.

After complete precipitation of $BaSO_4$, the fission-products solution was withdrawn and centrifuged to ensure that it became free from any traces of the $BaSO_4$ precipitate. Figure 3.14 (a and b) shows the gamma spectra of the fission-products solution before and after addition of the $BaCl_2$ solution and separation of the formed $BaSO_4$ precipitate. The precipitate was suspended in and washed by 40 % H_2SO_4, where it was transferred semi-quantitatively from the conical flask and filtered on a Whatman No. 1 filter paper to wash out (desorb) the adsorbed cations. Comparing the gamma spectra obtained in (a) and (b) of Figure 3.14 indicates that, addition of 20 mg $BaCl_2$ to the fission-products solution was sufficient for complete separation of ^{140}Ba and ^{140}La.

While the barium sulfate precipitate is white, the formed precipitate was pink (even after washing) this is due to coprecipitation of some $KMnO_4$ with $BaSO_4$ by forming a mixed crystal **(Nesmeyanov, 1974; Agasyan, 1980)**. The remaining $KMnO_4$ was still in the acidified fission-products solution as indicated by the pink color of the solution. Faster growth of the $BaSO_4$ precipitate crystals increases the coprecipitation by occlusions, in which ions of the solution can be adsorbed and trapped inside the crystal because these adsorbed ions may not be desorbed before the next larger crystal growth, and mechanical entrapment, in which a part of the solution may be entrapped as a result of the crystalline mass

formation by the several small crystals physically lying close together during the growth. The ions adsorbed by occlusions and/or mechanical entrapment cannot be removed by washing. On contrast, occlusions and mechanical entrapment can be minimized by slow precipitation from homogeneous solution **(Rengan et al., 1993)**. Thus in this work the fission-products solution was eventually allowed to stand until complete precipitation of $BaSO_4$.

3.5.2. Radiometric analysis of the formed precipitate:

Figure 3.15 shows the gamma spectrum of the formed $BaSO_4$ precipitate after washing with 40 % H_2SO_4. Table 3.8 compiles the nuclear and radiometric analysis data for the process of batch precipitation with $BaSO_4$. As shown in Figure 3.15, the formed barium sulfate precipitate contains (i) ^{90m}Y ($T_{1/2}$ = 3.19 h), (ii) ^{132}I, (iii) ^{137m}Ba ($T_{1/2}$ = 2.55 min), (iv) ^{140}Ba ($T_{1/2}$ = 12.75 d) and its daughter ^{140}La ($T_{1/2}$ = 1.68 d), (v) ^{141}Ce ($T_{1/2}$ = 32.5 d), (vi) ^{143}Ce ($T_{1/2}$ = 1.38 d), and (vii) ^{144}Ce ($T_{1/2}$ = 284.6 d).

^{132}I was carried down by the $BaSO_4$ precipitate by surface adsorption mechanism. The $BaSO_4$ precipitate contained only traces of both ^{132}I and ^{137m}Ba because of washing and volatilization of a great fraction of the former and rapid decay of the latter (a decay product of ^{137}Cs) due to its short half-life (2.55 min).

Disappearance of ^{140}La from the fission-products solution after precipitation of $BaSO_4$ indicated that ^{140}La itself was precipitated from the solution, i.e., only a fraction of ^{140}La found in the precipitate was produced from decay of ^{140}Ba after precipitation of $BaSO_4$, while the remaining of it was carried down from the fission-products solution during precipitation of $BaSO_4$. Presence of ^{140}La and ^{141}Ce in the $BaSO_4$ precipitate might be due to formation of the double salts $La_2(SO_4)_3.3Na_2SO_4.2H_2O$ and

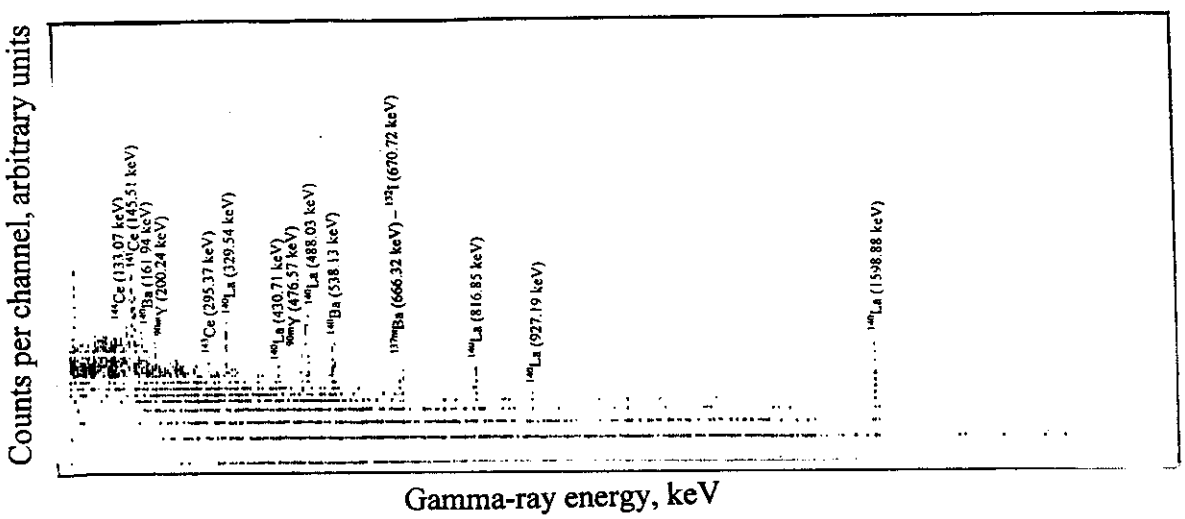

Figure 3.15. Gamma spectrum of the formed $BaSO_4$ precipitate after washing with 40 % H_2SO_4.

Table 3.8. Nuclear and radiometric analysis data for the process of batch precipitation with $BaSO_4$.

Isotope	Half-life, $T_{1/2}$	Fission yield, Y_f	Decay mode	Main γ-energy (abundance), and other γ-energies in keV	CTRDs of the obtained γ-photopeaks in keV		
					F.P solution		$BaSO_4$ precipitate
					Before adding $BaCl_2$ solution	After adding $BaCl_2$ solution	
^{90m}Y	3.19 h	5.78 %	I.T	202.51(96.6%), 479.53, ...	Not detected	Not detected	200.24, 476.57
^{132}I	Table 3.2				670.36, 525.1, 632.97, 775.37, 815.05, 957.03, 1296.74	669.62, 523.73, 631.55, 775.26, 815.33, 958.15	670.72
^{137m}Ba	2.55 min	5.85 %	I.T	661.6 (89.9 %) 624.2, 655.7	664.81	662.64	666.32
^{140}Ba	12.75 d	6.21 %	β^-	537.60 (24.4 %), 162.90, ...	539.27	Not detected	538.13, 161.94
^{140}La	1.68 d	6.22 %	β^-	1596.60 (95.4 %), 328.77, 432.55, 487.03, 815.83, 925.23, ...	1594.85, 815.05	Not detected	1598.88, 329.54, 430.71, 488.03, 816.85, 927.19
^{141}Ce	32.5 d	5.85 %	β^-	145.45 (48.3 %), 103.4, ...	Not detected	Not detected	145.51
^{143}Ce	1.38 d	5.96 %	β^-	293.2 (43.4 %), 664.59, 721.98, ...	Not detected	Not detected	295.37
^{144}Ce	284.6 d	5.5 %	β^-	133.53 (11 %), 80.12	Not detected	Not detected	133.07

$Ce_2(SO_4)_3.3Na_2SO_4.2H_2O$, respectively, in the acidified-fission products solution **(Mellor, 1960; Library of Congress, 1997)**. Since Na_2SO_4, in which these double salts are sparingly soluble, was present in the solution in very large amount relative to the double salts formed by lanthanum and cerium, these double salts came out from the solution **(Mellor, 1960; Cotton and Wilkinson, 1979)**, but they did not precipitate (because of their very low concentrations) until the barium carrier was added to carry them down with the formed $BaSO_4$ precipitate.

The isotopes appeared in the $BaSO_4$ precipitate (Figure 3.15) decay as follows:

1. ^{90m}Y ($T_{1/2}$ = 3.19 h) decays to its isomer ^{90}Y ($T_{1/2}$ = 2.67 d) which finally decays to stable ^{90}Zr.
2. ^{132}I, as mentioned before in Section 3.3 and shown in Figure 3.5 (b), decays to stable ^{132}Xe.
3. ^{137m}Ba decays to stable ^{137}Ba.
4. ^{140}Ba decays to ^{140}La which in turn decays to stable ^{140}Ce.
5. ^{141}Ce decays to stable ^{141}Pr.
6. ^{143}Ce decays to ^{143}Pr ($T_{1/2}$ = 13.57 d) which finally decays to stable ^{143}Nd.
7. ^{144}Ce decays to ^{144m}Pr ($T_{1/2}$ = 7.2 min) which decays to its isomer ^{144}Pr ($T_{1/2}$ = 17.28 min) which, in turn, decays to the pure α-emitter ^{144}Nd ($T_{1/2} = 2.1 \times 10^{15}$ y) which finally decays, via α-emission, to stable ^{140}Ce.

^{90}Y, ^{143}Pr, ^{144m}Pr, and ^{144}Pr isotopes did not appear in the gamma spectrum of $BaSO_4$ precipitate because of the low-abundance gamma rays of their decay; 1.4×10^{-6} % of 2186.24 keV for ^{90}Y, 1.2×10^{-6} % of 741.98 keV for ^{143}Pr, 0.08 % of 59.03 keV and 0.033 % of 1631.4 keV for ^{144m}Pr, and 1.3 % of 696.51 keV for ^{144}Pr. Figure 3.16 (a, b, c, d, and e) shows the decay chains of ^{90m}Y, ^{140}Ba, ^{141}Ce, ^{143}Ce, and ^{144}Ce as ^{235}U-fission products.

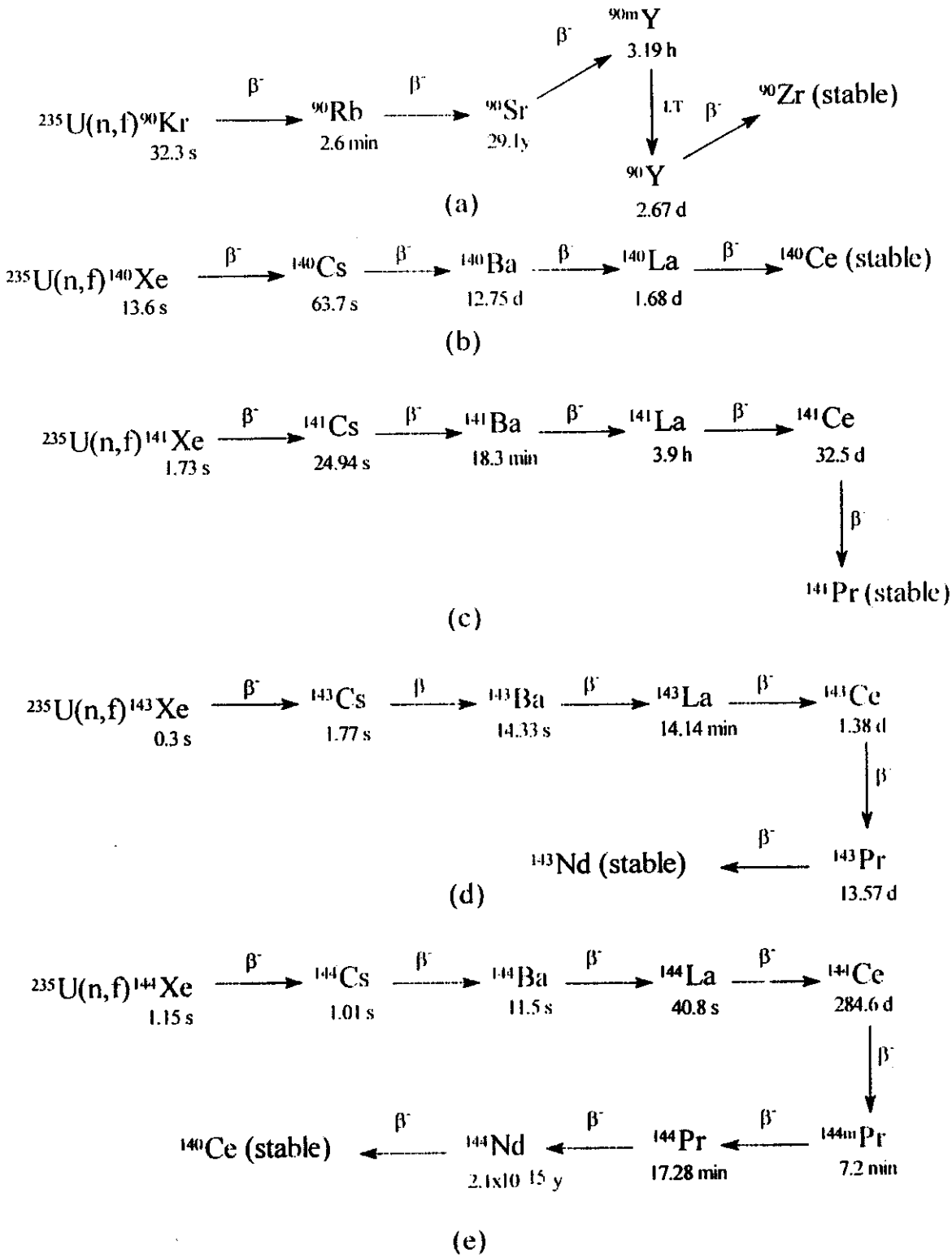

Figure 3.16. Decay chains of (a) ^{90m}Y, (b) ^{140}Ba, (c) ^{141}Ce, (d) ^{143}Ce, and (e) ^{144}Ce as ^{235}U-fission products.

In addition to ^{137m}Ba, ^{137}Ba, and ^{140}Ba, there are other eight ^{235}U-fission-barium isotopes; these are ^{135}Ba, ^{136}Ba, ^{138}Ba, ^{139}Ba, ^{141}Ba, ^{142}Ba, ^{143}Ba, and ^{144}Ba. Of these isotopes, ^{135}Ba, ^{136}Ba, and ^{138}Ba are stable ones. ^{139}Ba, ^{141}Ba, ^{142}Ba, ^{143}Ba, and ^{144}Ba are all short-lived isotopes with half-life periods of 1.4 h, 18.3 min, 10.7 min, 14.33 s, and 11.5 s, respectively. These five barium isotopes decayed completely during the seven-days cooling period.

In addition to the aforementioned ^{235}U-fission cerium isotopes (^{140}Ce, ^{141}Ce, ^{142}Ce, ^{143}Ce, and ^{144}Ce), there is a more short-lived one; ^{146}Ce ($T_{1/2}$ = 13.52 min), which decayed completely during the cooling time of seven-days.

Fission reactions of ^{235}U give rise to nine strontium isotopes, namely ^{86}Sr, ^{87}Sr, ^{88}Sr, ^{89}Sr, ^{90}Sr, ^{91}Sr, ^{92}Sr, ^{93}Sr, and ^{94}Sr. Of these isotopes, ^{86}Sr, ^{87}Sr, and ^{88}Sr are stable ones. Strontium-89 has a half-life period of 50.52 d, while the longest-lived fission-strontium isotope, ^{90}Sr, has a half-life period of 29.1 y. The isotopes of ^{91}Sr, ^{92}Sr, ^{93}Sr, and ^{94}Sr are short-lived isotopes with half-life periods of 9.5 h, 2.71 h, 7.4 min, and 75.2 s, respectively, so that these isotopes decayed completely during the seven-days cooling period. Strontium-89 decays to stable ^{89}Y, whereas ^{90}Sr, as shown in Figure 3.16 (a), decays to ^{90m}Y. Strontium-89 has low-abundance gamma-rays of decay (0.01 % of 909.1 keV), while ^{90}Sr is a pure β^--emitter so that both of these two isotopes did not appear neither in gamma spectrum of the $BaSO_4$ precipitate nor in any other gamma spectra in this work. Presence of ^{90}Sr in the $BaSO_4$ precipitate was confirmed by appearance of its daughter (^{90m}Y) in the gamma spectrum of the precipitate (where ^{90m}Y found in the $BaSO_4$ precipitate was produced from the decay of ^{90}Sr after precipitation).

Table 3.9 compiles the nuclear characteristics and fission yields of the barium, lanthanum, cerium, yttrium, and strontium isotopes produced from fission reactions of ^{235}U.

Table 3.9. Nuclear characteristics and fission yields of the ^{235}U-fission barium, lanthanum, cerium, strontium, and yttrium isotopes.

Isotope		Half-life, $T_{1/2}$	Fission yield, Y_f	Decay mode	Main γ-energy (abundance), and other γ-energies in keV
Barium isotopes	^{135}Ba	Stable		-	-
	^{136}Ba	Stable	0.0062 %	-	-
	^{137m}Ba	Table 3.8			
	^{137}Ba	Stable	5.85 %	-	-
	^{138}Ba	Stable	6.71 %	-	-
	^{139}Ba	1.4 h	6.41 %	β^-	165.85 (23.7 %), 126.9, 1420.5, ...
	^{140}Ba	Table 3.8			
	^{141}Ba	18.3 min	5.83 %	β^-	190.33 (46 %), 276.95, 304.18, ...
	^{142}Ba	10.7 min	5.75 %	β^-	255.12 (21.1 %), 895.2, 1204.3, ...
	^{143}Ba	14.33 s	5.55 %	β^-	211.5 (6.6 %), 798.7, 1010.7, ...
	^{144}Ba	11.5 s	4.4 %	β^-	103.9 (25 %), 388.2, 430.5, ...
Lanthanum isotopes	^{139}La	Stable	6.41 %	-	-
	^{140}La	Table 3.8			
	^{141}La	3.9 h	5.85 %	β^-	1354.5 (1.6 %), 1693, 2267, ...
	^{142}La	1.54 min	5.85 %	β^-	641.21 (47.4 %), 2389, 2542.9, ...
	^{143}La	14.14 min	5.92 %	β^-	620.5 (1.5 %), 6[illegible]3.7, 798.5, ...
Cerium isotopes	^{140}Ce	Stable	6.22 %	-	-
	^{141}Ce	Table 3.8			
	^{142}Ce	Stable	5.85 %	-	-
	^{143}Ce	Table 3.8			
	^{144}Ce	Table 3.8			
	^{146}Ce	13.52 min	2.99 %	β^-	316.8 (52.5 %), 218.3, 133.6, , ...
Strontium isotopes	^{86}Sr	Stable	~ 3.1×10^{-5} %	-	-
	^{87}Sr	Stable	2.7 %	-	-
	^{88}Sr	Stable	3.58 %	-	-
	^{89}Sr	50.52 d	4.73 %	β^-	909.1 (0.01 %), 891.9, 906.6
	^{90}Sr	29.1 y	5.78 %	β^-	-
	^{91}Sr	9.5 h	5.83 %	β^-	1024.25 (33.5 %), 652.98, 749.77, ...
	^{92}Sr	2.71 h	5.94 %	β^-	1383.94 (93.3 %), 430.56, 953.32, ...
	^{93}Sr	7.4 min	6.24 %	β^-	590.28 (67.2 %), 875.73, 888.13, ...
	^{94}Sr	75.2 s	6.06 %	β^-	1427.7 (94 %),723.8, 621.7, 703.9, ...
Yttrium isotopes	^{89}Y	Stable	4.73 %	-	-
	^{90m}Y	Table 3.8			
	^{90}Y	2.67 d	5.78 %	β^-	2186.24 (1.4×10^{-6} %), 1760.7
	^{91m}Y	49.71 min	2.332 %	I.T, β^-	555.57 (95 %)
	^{91}Y	58.51 d	5.83 %	β^-	1204.77 (0.3 %)
	^{92}Y	3.54 h	5.94 %	β^-	934.44 (13.7 %), 448.5, 1405.44, ...
	^{93}Y	10.2 h	6.24 %	β^-	267.05 (6.8 %), 680.25, 947.07, ...
	^{95}Y	10.3 min	6.38 %	β^-	954.2 (18.8 %), 2176, 3577.1, ...

3.6. Batch separation of Zr, Nb, Te, and Np radionuclides:

3.6.1. Separation technique:

After separation of the formed $BaSO_4$ precipitate, the fission-products solution was transferred to another conical flask. Solution of $FeCl_3$, dissolved in 1 M HCl acid, was added to the fission-products solution dropwise with stirring to attain homogeneity. In such case, the following reaction occurs:

$$2FeCl_3 + 3H_2SO_4 \longrightarrow Fe_2(SO_4)_3 + 6HCl$$

After adding the $FeCl_3$ solution, the fission-products solution was left to withstand for ~15 min. Then, the pH-value was raised gradually and slowly (to minimize occlusions and mechanical entrapment) until it reached ~7. For complete settling of the formed $Fe_2O_3.nH_2O$ precipitate, the solution was left for about one hour. During raising pH-value of the fission-products solution, the remaining manganese precipitated as MnO_2 at pH = 3.5 according to the following redox reaction **(Cotton and Wilkinson, 1979; Carus Chemical Company, 1997)**:

$$MnO_4^- + 2H_2O + 3e^- = MnO_2\downarrow + 4OH^-$$

Complete precipitation of aluminum as $Al(OH)_3$ was achieved as the pH reached ~5 **(Agasyan, 1980)**. After complete settling of the $Fe_2O_3.nH_2O$ precipitate, the fission-products solution was withdrawn and centrifuged to ensure that it became free from any traces of the $Fe_2O_3.nH_2O$ precipitate. Figure 3.17 (a and b) shows the gamma spectra of the fission-products solution before and after addition of 20 mg $FeCl_3$ and separation of the formed $Fe_2O_3.nH_2O$ precipitate. The precipitate was suspended in and washed by distilled water, where it was transferred semi-quantitatively

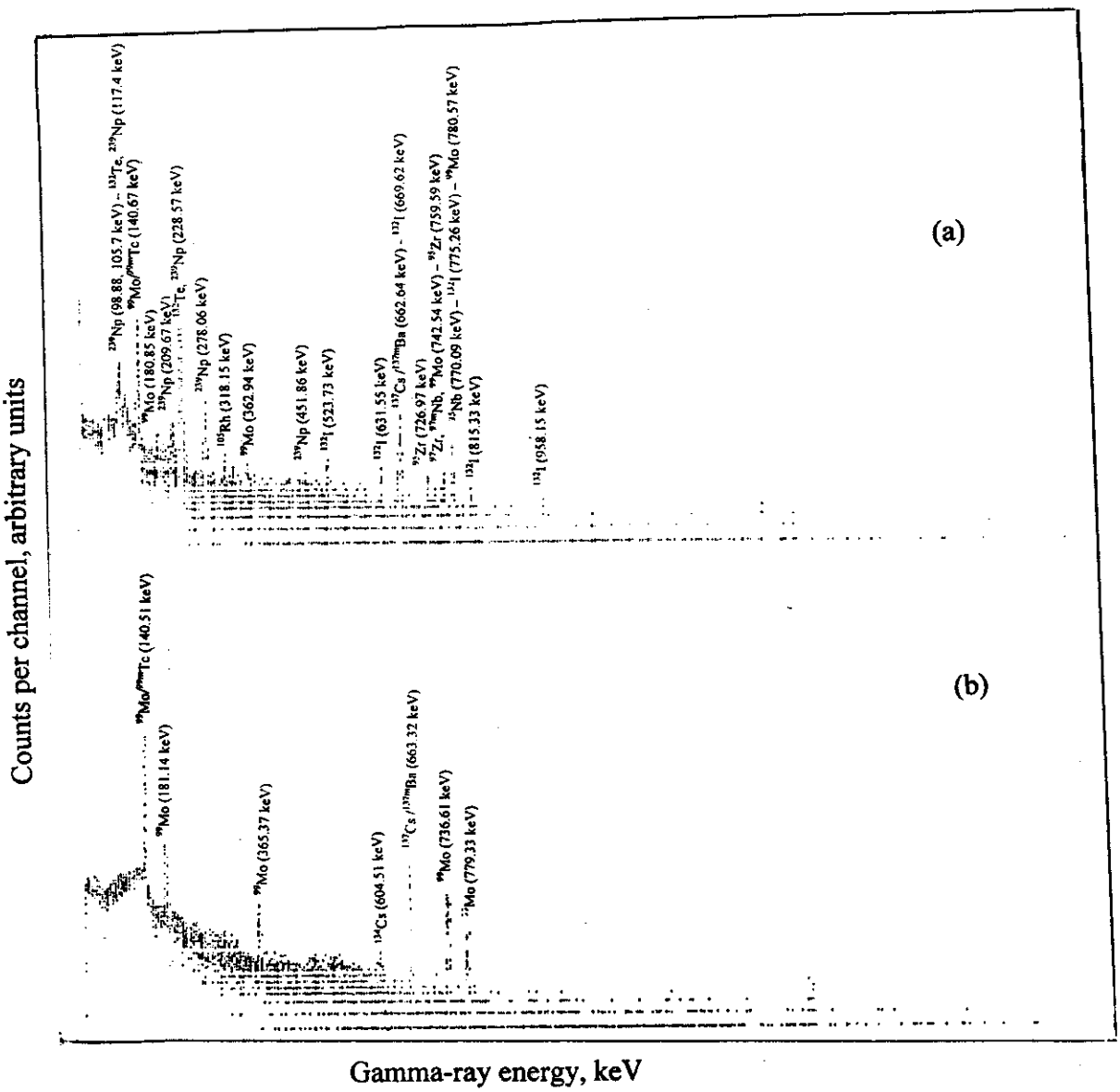

Figure 3.17. Gamma spectra of the fission-products solution (a) before addition of the $FeCl_3$ and (b) after addition of $FeCl_3$ and separation of the formed precipitate.

from the conical flask and filtered on a Whatman No. 1 filter paper. Comparing the gamma spectra obtained in (a) and (b) of Figure 3.17, indicates complete disappearance of ^{95}Zr, ^{97}Zr, ^{95}Nb, ^{97m}Nb, ^{97}Nb, ^{105}Rh, ^{132}Te, ^{132}I, and ^{239}Np from the fission-products solution after addition of 20 mg $FeCl_3$ and separation of the formed $Fe_2O_3.nH_2O$ precipitate at pH-value of ~ 7.

One of the most conspicuous features of ferric iron in aqueous solutions is its tendency to hydrolyze and/or to form complexes. It has been established that hydrolysis (equivalent in the first stage to acid dissociation of the aquo ion) is governed in its initial stages by the following equilibrium constants:

$$[Fe(H_2O)_6]^{3+} = [Fe(H_2O)_5(OH)]^{2+} + H^+ \qquad k = 10^{-3.05}$$

$$[Fe(H_2O)_5(OH)]^{2+} = [Fe(H_2O)_4(OH)_2]^{+} + H^+ \qquad k = 10^{-3.26}$$

$$2[Fe(H_2O)_6]^{3+} = [Fe(H_2O)_4(OH)_2Fe(H_2O)_4]^{4+} + 2H^+ \qquad k = 10^{-2.91}$$

In the last of these equations the binuclear species is believed to have the structure:

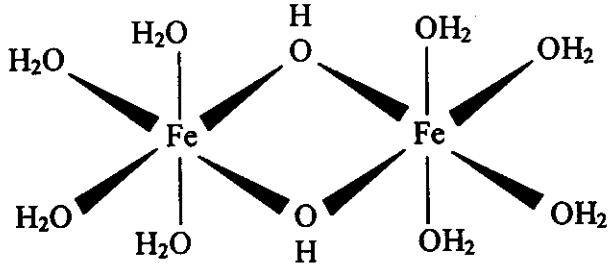

Even at the rather acid pH's of 2-3, the extent of hydrolysis is very great. In order to have solutions containing Fe^{3+} mainly (~99 %) in the form of the pale purple hexaquo ion, the pH must be around zero. As the pH-value is raised above 2-3, more highly condensed species than the binuclear one shown above are formed. The attainment of equilibrium becomes sluggish,

and some colloidal gels are formed. Ultimately hydrous ferric oxide $Fe_2O_3.nH_2O$ (which, with no evidence, commonly called ferric hydroxide) is precipitated as a red-brown gelatinous mass. At least a part of such precipitates seems to be the FeO(OH) **(Cotton and Wilkinson, 1979)**. Complete precipitation of the Fe^{3+} ion occurs at pH = 3.5. In an ammoniacal solution, particles of the precipitate are positively charged as a result of adsorption of OH^- ions, acquiring a negative charge and therefore on coagulation carry down various cations. Conversely, In a weakly acid medium, particles of the precipitate are positively charged because of adsorption of the species $Fe(OH)_2^+$ or $Fe(OH)^{2+}$ and, as a result, it adsorbs various anions from the solution **(Agasyan, 1980)**. Since it has a very large surface area, hydrous ferric oxide is used as a scavenger, where it scavenges actinides and many other elements by incorporating them into its gelatinous matrix **(Glasstone, 1955; NEA, 1997)**.

3.6.2. Radiometric analysis of the formed precipitate:

Figure 3.18 shows the gamma spectrum of the formed $Fe_2O_3.nH_2O$ precipitate after washing with distilled water. Table 3.10 compiles the nuclear and radiometric analysis data for the process of batch precipitation with $Fe_2O_3.nH_2O$.

According to Figure 3.18, it was found that the hydrous ferric oxide precipitate contained (i) ^{95}Zr ($T_{1/2}$ =64.02 d) and its daughter ^{95}Nb ($T_{1/2}$ = 34.97 d), (ii) ^{97}Zr ($T_{1/2}$ =16.9 h), its daughter ^{97m}Nb ($T_{1/2}$ = 58.1 s), and its granddaughter ^{97}Nb ($T_{1/2}$ = 1.23 h), (iii) ^{105}Rh ($T_{1/2}$ = 35.36 h), (iv) ^{132}Te ($T_{1/2}$ = 3.26 d) and its daughter ^{132}I, and (v) ^{239}Np ($T_{1/2}$ =2.36 d). Coprecipitation of these isotopes with the hydrous ferric oxide precipitate can be elucidated as follows:

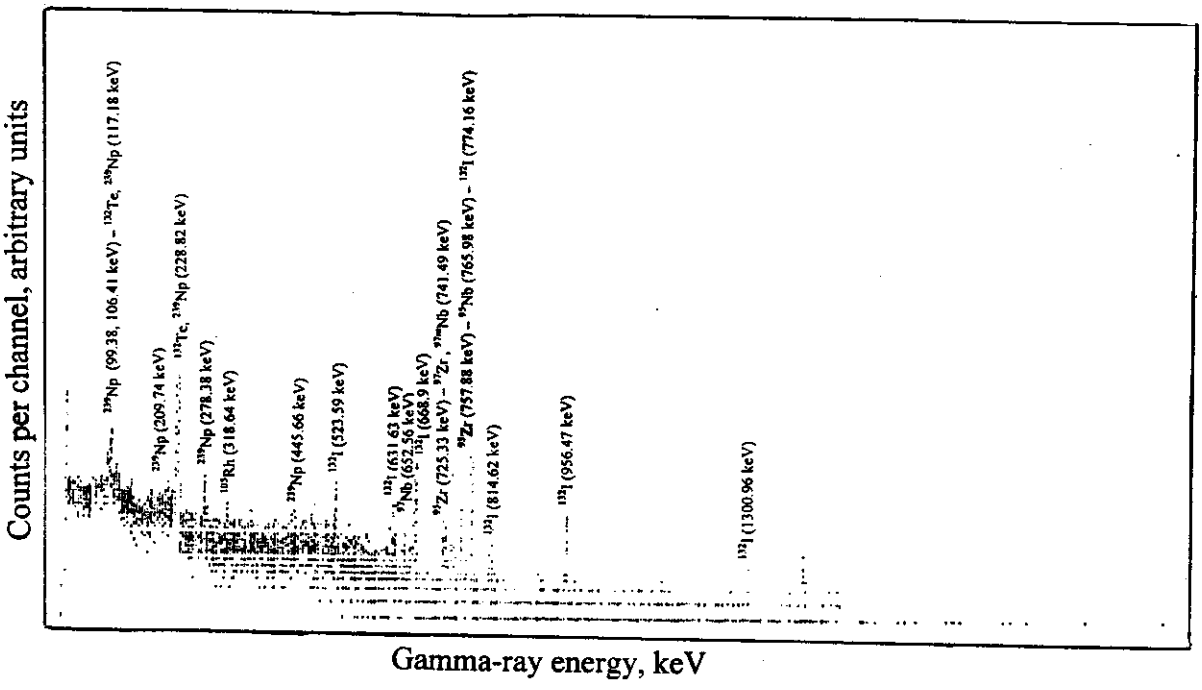

Figure 3.18. Gamma spectrum of the formed $Fe_2O_3.nH_2O$ precipitate after washing with distilled water.

Table 3.10. Nuclear and radiometric analysis data for the process of batch precipitation with $Fe_2O_3.nH_2O$.

Isotope	Half-life, $T_{1/2}$	Fission yield, Y_f	Decay mode	Main γ-energy (abundance), and other γ-energies in keV	CTRDs of the obtained γ-photopeaks in keV		
					F.P solution		$Fe_2O_3.nH_2O$ Precipitate
					Before adding $FeCl_3$ solution	After adding $FeCl_3$ solution	
^{95}Zr	64.02 d	6.5 %	β^-	756.87 (54.6 %), 724.24, ...	759.59, 726.97	Not detected	757.88, 725.33
^{97}Zr	16.9 h	5.98 %	β^-	743.5 (92.8 %), 507.63, ...	742.54	Not detected	741.49
^{95}Nb	34.97 d	6.5 %	β^-	765.84 (99.8), 745.8, ...	770.09	Not detected	765.98
^{97m}Nb	58.1 s	5.63 %	I.T	743.3 (97.9 %)	742.54	Not detected	741.49
^{97}Nb	1.23 h	6 %	β^-	657.92 (98.3 %), 1024	Not detected	Not detected	652.56
^{105}Rh	Table 3.5				318.15	Not detected	318.64
^{132}Te	3.26 d	4.31 %	β^-	228.16 (88 %), 116.30, ...	228.57, 117.4	Not detected	228.82, 117.18
^{132}I	Table 3.2				669.62, 523.73, 631.55, 775.26, 815.33, 958.15	Not detected	668.9, 523.59, 631.63, 814.62, 956.47, 1300.96
^{239}Np	2.36 d	Not a fission product	β^-	106.4 (22.8 %), 99.5, 103.7, 209.8, 228.1, 277.9, 447.6, ...	105.7, 98.88, 117.4, 209.67, 228.57, 278.06, 451.86	Not detected	106.41, 99.38, 117.18, 209.74, 228.82, 278.38, 445.66

Zirconium isotopes (^{95}Zr and ^{97}Zr). In the acidified fission-products solution, zirconium was in the form of $ZrSO_4.nH_2O$, where n = 4, 5, or 7 **(Cotton and Wilkinson, 1979; Etherington, 1958)**. Generally in the aqueous acidic solutions, Zr(IV) compounds present as partly hydrolyzed species, e.g., $[Zr_3(OH)_4]^{8+}$ and $[Zr_4(OH)_8]^{8+}$. Addition of a hydroxide to Zr(IV) solutions causes precipitation of the white gelatinous compound $ZrO_2.nH_2O$ **(Housecroft and Sharpe, 2001)**. Thus during raising pH of the solution, zirconium might be coprecipitated with $Fe_2O_3.nH_2O$ as $ZrO_2.nH_2O$ in the pH-range 1.5-2 **(Morozova et al., 1989)**. On the other hand, **Kolenkova et al. (1980)** recommended carrying out of the preliminary precipitation of Zr, Fe, Al at pH = 4.5.

Niobium isotopes (^{95}Nb, ^{97m}Nb, and ^{97}Nb). The oxidation state of +5 is the most common one for niobium in its compounds, lower oxidation states are less stable. Niobium(V) might exist in a variety of species at equilibrium in the acidified-fission products solution, e.g., $[Nb_2O(SO_4)]^{6+}$ and $Nb_2O_2(SO_4)_3$ **(Cotton and Wilkinson, 1979; Greenwood and Earnshaw, 1984)**. The hydrous niobium(V) oxide precipitate, $Nb_2O_5.nH_2O$, is obtained upon neutralization of the Nb(V)-acid solutions **(Cotton and Wilkinson, 1979)**. Thus, on raising the pH-value of the solution to ~5, $Nb_2O_5.nH_2O$ coprecipitates with $Fe_2O_3.nH_2O$ and it becomes quantitatively precipitated as the pH-value is raised above 6 **(Margalit and Seyeda, 2000)**.

Rhodium-105. Rhodium existed in the acidified fission-products solution in the form of the stable aquo ion $[Rh(H_2O)_6]^{3+}$ **(Cotton and Wilkinson, 1979)**. Generally, $Rh_2O_3.5H_2O$ precipitates when alkali is added to the Rh(III) solutions **(Greenwood and Earnshaw, 1984)**. Thus, rhodium was coprecipitated with $Fe_2O_3.nH_2O$ as $Rh_2O_3.5H_2O$ at pH =7.

Tellurium-132. Orthotelluric acid, $Te(OH)_6$, can be prepared by oxidation of tellurium or TeO_2 by H_2O_2, Na_2O_2, CrO_3, or other powerful

oxidizing agents (**Cotton and Wilkinson, 1979; Aggarwal, 1987**), Thus upon adding H_2O_2, which was added during acidification of the fission-products solution before separation of ^{131}I, $Te(OH)_6$ might be formed. $Te(OH)_6$ is insensitive to concentration, temperature, and acidic pH. In basic pH-range of 6 to 10, $Te(OH)_6$ precipitate is formed (**Minter and Iriarte-Gross, 2000**).

Neptunium-239. Neptunium species, of oxidation numbers lower than VI, in the acidified fission-products solution were oxidized by $KMnO_4$ to Np(VI) (**Nesmeyanov, 1974; 1984**). During raising pH-value of the solution, neptunium(VI) coprecipitated with $Fe_2O_3.nH_2O$ as $NpO_2(OH)_2$ in the pH-range 2-3 (**Ahrland et al., 1975**).

The isotopes appeared in the gamma spectrum of the $Fe_2O_3.nH_2O$ precipitate have the following decay routes:

1. ^{105}Rh decays to stable ^{105}Pd.
2. ^{132}Te decays to ^{132}I which in turn decays to stable ^{132}Xe (Figure 3.5, b and Section 3.3).
3. 1.4 % of ^{95}Zr decays to ^{95m}Nb ($T_{1/2}$ = 3.61 d), which in turn decays to ^{95}Nb, which finally decays to stable ^{95}Mo, whereas 98.6 % of ^{95}Zr decays directly to ^{95}Nb. ^{95m}Nb did not appear in any of the gamma spectra of this work because it has low fission yield (Y_f = 0.0651 %).
4. More than 95 % of ^{97}Zr decays to ^{97m}Nb ($T_{1/2}$ = 58.1 s), which in turn decays to ^{97}Nb ($T_{1/2}$ = 1.23 h), which finally decays to stable ^{97}Mo, whereas less than 5 % of ^{97}Zr decays directly to ^{97}Nb.

Fission reactions of uranium-235 give rise to other six zirconium isotopes, in addition to ^{95}Zr and ^{97}Zr; ^{93}Zr ($T_{1/2} = 1.53 \times 10^6$ y) and the stable isotopes ^{90}Zr, ^{91}Zr, ^{92}Zr, ^{94}Zr, and ^{96}Zr. Zirconium-93 decays to ^{93m}Nb ($T_{1/2}$ = 16.13 y) which in turn decays to stable ^{93}Nb. Both of ^{93}Zr and ^{93m}Nb did not appear in any of the gamma spectra of this work because of their low-energy characteristic gamma rays of decay (30.77 keV for both).

In addition to ^{132}Te, there are other 15 ^{235}U-fission tellurium isotopes; ^{125m}Te, ^{125}Te, ^{126}Te, ^{127m}Te, ^{127}Te, ^{128}Te, ^{129m}Te, ^{129}Te, ^{130}Te, ^{131m}Te, ^{131}Te, ^{133m}Te, ^{133}Te, ^{134}Te, and ^{135}Te. Of these tellurium isotopes, only three ones are stable; these are ^{125}Te, ^{126}Te, and ^{128}Te. The short-lived isotopes ^{133m}Te ($T_{1/2}$ = 55.4 min), ^{133}Te ($T_{1/2}$ = 12.4 min), ^{134}Te ($T_{1/2}$ = 41.8 min), and ^{135}Te ($T_{1/2}$ =19 s) decayed completely during the seven-days cooling period. The isotopes of ^{125m}Te, ^{127m}Te, ^{129m}Te, and ^{130}Te decay as follows:

1. ^{125m}Te ($T_{1/2}$ = 58 d) decays to stable ^{125}Te.
2. ^{127m}Te ($T_{1/2}$ = 109 d) decays to ^{127}Te ($T_{1/2}$ = 9.4 h) which in turn decays to the aforementioned stable ^{127}I.
3. ^{129m}Te ($T_{1/2}$ = 33.6 d) decays to ^{129}Te which in turn decays to the aforementioned ^{129}I, which finally decays to stable ^{129}Xe.
4. ^{130}Te ($T_{1/2} = 2.5 \times 10^{21}$ y) decays to stable ^{130}Xe.
5. ^{131m}Te ($T_{1/2}$ =1.35 d) decays to ^{131}Te ($T_{1/2}$ = 25 min) which in turn decays to the aforementioned ^{131}I (Figure 3.5, a and Section 3.3).

Tellurium-130 is a pure β^--emitter. The isotopes of ^{125m}Te, ^{127m}Te, ^{127}Te, ^{129m}Te, ^{129}Te, and ^{131m}Te did not appear in any of the obtained gamma spectra of this work either because of (i) low-abundance gamma rays of decay, (ii) low fission-yield, or (iii) a combination of both (i) and (ii). Fission yields of these tellurium isotopes are 0.0077 %, 0.025 %, 0.156 %, 0.09 %, 0.511%, and 0.412 % respectively, whereas abundances of their main gamma rays of decay are 6.7 % of 35.46 keV for ^{125m}Te, 0.3 % of 57.63 keV for ^{127m}Te, 0.9 % of 417.9 keV for ^{127}Te, 4.9 % of 695.98 keV for ^{129m}Te, 17.6 % of 27.8 keV and 8 % of 458.6 keV for ^{129}Te, and 38.6 % of 773.7 keV for ^{131m}Te. Tellurium-131 (Y_f = 2.89 %) did not also appear in the gamma spectra because, as shown in Figure 3.5 (a), the greater fraction of ^{131}Te is produced from direct decay of ^{131}Sb ($T_{1/2}$ = 23.03 min) which decayed completely during the cooling time of seven days. 91.6 % of ^{131}Sb decays directly to ^{131}Te, while only 8.4 % of ^{131}Sb decays first to ^{131m}Te.

Figure 3.19 (a, b, and c) shows the decay chains of ^{95}Zr, ^{97}Zr, and ^{105}Rh as ^{235}U-fission products, while Table 3.11 compiles the nuclear characteristics and fission yields of the zirconium, niobium, and tellurium isotopes produced from fission reactions of ^{235}U.

^{237}Np ($T_{1/2}$ = 2.14 × 10^6 y) and ^{239}Np ($T_{1/2}$ = 2.355 d) are obtained upon irradiating natural uranium targets, but they are not fission products. When the uranium target is bombarded in a nuclear reactor by fast neutrons, weighable amounts of ^{237}Np are formed by the nuclear reactions:

$$^{238}U\,(n, 2n)^{237}U \xrightarrow[6.75\ d]{\beta^-} {}^{237}Np$$

$$^{235}U(n,\gamma)^{236}U(n,\gamma)^{237}U \xrightarrow[6.75\ d]{\beta^-} {}^{237}Np$$

Thus, yield of ^{237}Np obtained by neutron-irradiation of uranium targets depends on the ratio of the fast neutrons in the reactor; the yield increases by increasing this ratio. Also, at short irradiation times the amount of ^{237}Np is low **(Nesmeyanov, 1974)**. ^{239}Np is the major activation product of ^{238}U **(Wu et al., 1995)** and it is produced via the irradiation reaction:

$$^{238}U(n,\gamma)^{239}U \xrightarrow[23.5\ min]{\beta^-} {}^{239}Np$$

Yield of ^{239}Np obtained by irradiation of, for example, 1 g of uranium for 24 h in a reactor with a flux of 10^{13} $n.cm^{-2}.s^{-1}$ is approximately 0.1 Ci **(Nesmeyanov, 1974)**. Both of ^{237}Np and ^{239}Np have long decay chains, in which the isotopes decay mainly by emitting α and β^- particles. Some isotopes in these decay chains (e.g., ^{225}Ra, ^{225}Ac, ^{227}Th, and ^{231}Pa etc) have low-abundance and/or low-energy gamma rays of decay. There are also

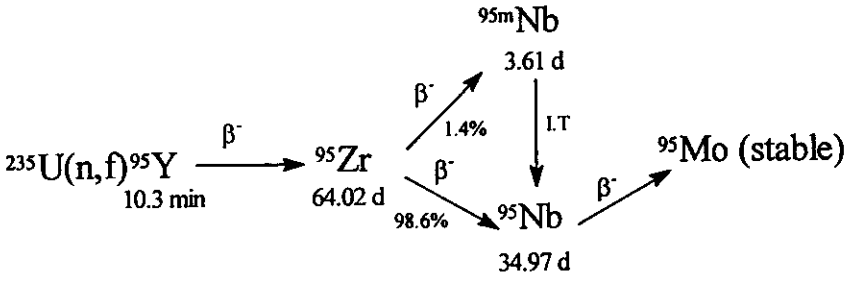

(a)

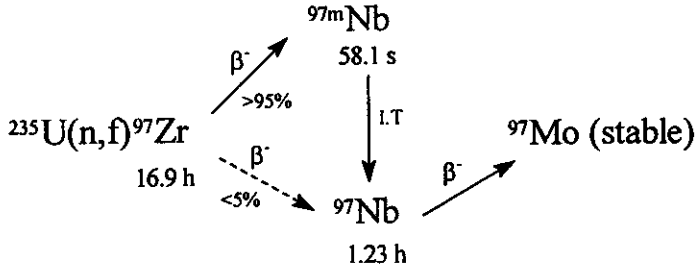

(b)

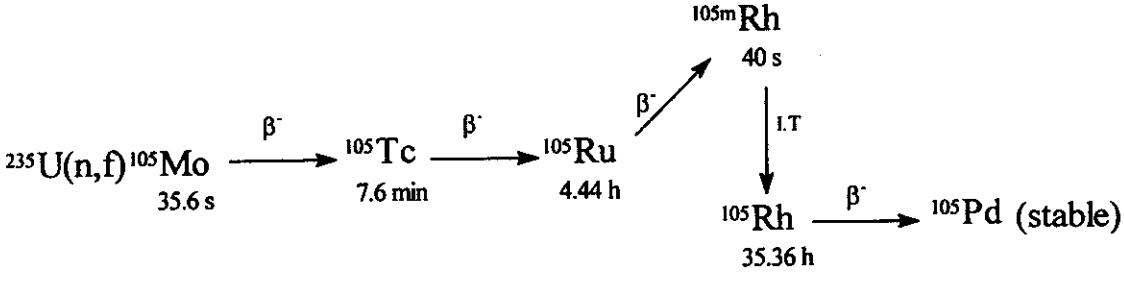

(c)

Figure 3.19. Decay chains of (a) ^{95}Zr, (b) ^{97}Zr, and (c) ^{105}Rh as ^{235}U-fission products.

Table 3.11. Nuclear characteristics and fission yields of the ^{235}U-fission zirconium, niobium, and tellurium isotopes.

Isotope		Half-life, $T_{1/2}$	Fission yield, Y_f	Decay mode	Main γ-energy (abundance), and other γ-energies in keV
Zirconium isotopes	^{90}Zr	Stable	5.9 %	-	-
	^{91}Zr	Stable	5.9 %	-	-
	^{92}Zr	Stable	6.1 %	-	-
	^{93}Zr	1.53×10^{6} y	6.35 %	β^-	30.77 (8.9×10^{-4} %)
	^{94}Zr	Stable	6.47 %	-	-
	^{95}Zr	Table 3.10			
	^{96}Zr	Stable	6.4 %	-	-
	^{97}Zr	Table 3.10			
Niobium isotopes	^{93m}Nb	16.13 y	6.03 %	I.T	30.77 (6×10^{-4} %), 30.3, ...
	^{93}Nb	Stable	6.03 %	-	-
	^{95m}Nb	3.61 d	0.0651 %	I.T, β^-	216.7 (48.59 %), 233, 235.7, ...
	^{95}Nb	Table 3.10			
	^{97m}Nb	Table 3.10			
	^{97}Nb	Table 3.10			
Tellurium isotopes	^{125m}Te	58 d	0.0077 %	I.T	35.46 (6.7 %), 109.27, 104.3, ...
	^{125}Te	Stable	0.034 %	-	-
	^{126}Te	Stable	0.059 %	-	-
	^{127m}Te	109 d	0.025 %	I.T, β^-	57.63 (0.3 %), 56.45, 87.25, ...
	^{127}Te	9.4 h	0.156 %	β^-	417.9 (0.9 %), 202.9, 360.3, ...
	^{128}Te	Stable	0.349 %	-	-
	^{129m}Te	33.6 d	0.09 %	I.T, β^-	695.98 (4.9 %), 105.5, 729.62, ...
	^{129}Te	1.16 h	0.511%	β^-	27.8 (17.6 %), 459.6, ...
	^{130}Te	2.5×10^{21} y	1.81 %	β^-	-
	^{131m}Te	1.35 d	0. 412%	I.T, β^-	773.7 (38.6 %), 793.8, 852.3, ...
	^{131}Te	25 min	2.89 %	β^-	149.8 (68.9 %), 452.4, 1147.4, ...
	^{132}Te	Table 3.10			
	^{133m}Te	55.4 min	3.99 %	I.T, β^-	912.58 (62.8 %), 647.6, 863.91, ...
	^{133}Te	12.4 min	3.06 %	β^-	312.08 (72.6 %), 407.63, 1333.21, ...
	^{134}Te	41.8 min	6.97 %	β^-	767.2 (29.9 %), 210.47, 278, ...
	^{135}Te	19 s	3.34 %	β^-	603 (100 %), 267, 870, ...

isotopes in these decay chains which may undergo further nuclear reactions such as (n,f) reactions (e.g., ^{233}U, ^{235}U and ^{239}Pu).

3.7. Production of radiocesium:

Figure 3.2 (a) indicates presence of the main γ-photopeak of ^{137}Cs, as its daughter ^{137m}Ba, (662.44 keV). There are 11 cesium isotopes produced from fission reactions of ^{235}U; ^{133}Cs, ^{135}Cs, ^{136}Cs, ^{137}Cs, ^{138}Cs, ^{139}Cs, ^{140}Cs, ^{141}Cs, ^{142}Cs, ^{143}Cs, and ^{144}Cs. Of these isotopes only ^{133}Cs is stable. The short-lived isotopes of ^{138}Cs ($T_{1/2}$ = 32.2 min), ^{139}Cs ($T_{1/2}$ = 9.3 min), ^{140}Cs ($T_{1/2}$ = 63.7 s), ^{141}Cs ($T_{1/2}$ = 24.94 s), ^{142}Cs ($T_{1/2}$ = 1.68 s), ^{143}Cs ($T_{1/2}$ = 1.77 s), and ^{144}Cs ($T_{1/2}$ = 1.01 s) decayed completely during the seven-days cooling period. ^{135}Cs ($T_{1/2}$ = 2.3 × 10^6 y), the daughter of ^{135m}Cs is a pure β^--emitter and decays to stable ^{135}Ba. Cesium-136 ($T_{1/2}$ = 13.16 d) decays to stable ^{136}Ba while, ^{137}Cs ($T_{1/2}$ = 30.17 y) decays to ^{137m}Ba ($T_{1/2}$ = 2.55 min) which in turn decays to stable ^{137}Ba. In addition to the aforementioned fission-cesium isotopes, ^{134}Cs ($T_{1/2}$ = 2.06 y) is produced during neutron-irradiation of uranium targets via the following activation reaction **(STUK, 2000)**:

$$^{133}Cs\ (n,\gamma)\ ^{134}Cs \xrightarrow[2.06\,y]{\beta^-} {}^{134}Ba\ (stable)$$

Figure 3.20 (a and b) shows the decay chains of ^{136}Cs and ^{137}Cs as ^{235}U-fission products, while Table 3.12 compiles the nuclear characteristics of ^{235}U-fission cesium isotopes and activation ^{134}Cs. Nuclear fission reaction is the primary and major means of producing ^{137}Cs, which is not a naturally occurring radionuclide. In other words, the largest source of ^{137}Cs and, therefore, the largest potential for waste material is from nuclear reactors and the large inventory of ^{137}Cs stored in irradiated fuel. ^{137}Cs is

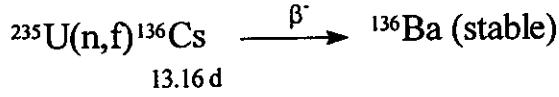

(a)

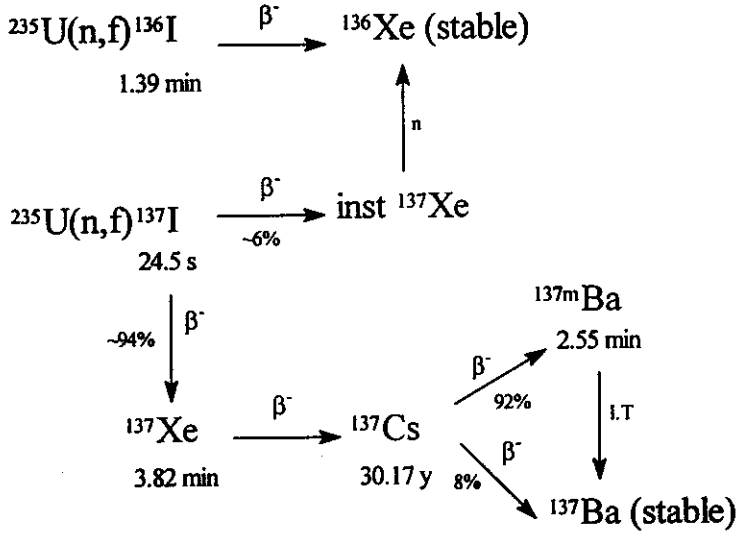

(b)

Figure 3.20. Decay chains of (a) ^{136}Cs and (b) ^{137}Cs as ^{235}U-fission products.

Table 3.12. Nuclear characteristics of the ^{235}U-fission cesium isotopes and ^{134}Cs.

Isotope	Half-life, $t_{1/2}$	Fission yield, Y_f	Decay mode	Main γ-energy (abundance), and other γ-energies in keV
^{133}Cs	Stable	6.5 %	-	-
^{134}Cs	2.065 y	Not a fission Product	β^-, E.C	604.74 (98.1 %), 605.65, 795.8, 796.47, ...
^{135}Cs	2.3×10^6 y	6.54 %	β^-	-
^{136}Cs	13.16 d	0.0062 %	β^-	818.5 (99.7 %), 340.6, 1048, ...
^{137}Cs	30.17 y	6.19 %	β^-	661.64 (86 %), 624.2, 655.7, ...
^{138}Cs	32.2 min	6.71 %	β^-	1435.86 (76.3 %), 462.79, 1009.78, ...
^{139}Cs	9.3 min	6.35 %	β^-	1283.2 (7.3 %), 627.3, ...
^{140}Cs	63.7 s	5.72 %	β^-	602.32 (55.6 %), 908.36, 1200.49, ...
^{141}Cs	24.94 s	4.17 %	β^-	48.48 (9.3 %), 555.74, 561.51, ...
^{142}Cs	1.68 s	2.72 %	β^-	1326.46 (12.92 %), 359.6, 966.9, ...
^{143}Cs	1.77 s	1.45 %	β^-	232.42 (8.32 %),306.42, 660.06, ...
^{144}Cs	1.01 s	0.423 %	β^-, β^--n	199.33 (100 %), 559.57, 639, ...

produced in a high yield from fission reaction of ^{235}U (Y_f = 6.19 %). It emits high-energy beta particles (944 keV), and is characterized also by emission of the 661.64 keV-gamma rays (86 %). Because of this high gamma-ray energy, ^{137}Cs has been used to sterilize medical supplies and to irradiate food **(Tingey et al., 1990)**. Another industrial applications of ^{137}Cs include (i) production of the plastic shrink tubing (irradiated plastic has the tendency to shrink after being heated), (ii) radiography to inspect metal castings and welds for flaws and material defects (e.g., cracks in steel pipes), (iii) sealed sources (containing known amounts of gamma radioactivity) for calibration (e.g., calibrating gamma-ray spectrometers and dose calibrators), and (iv) radioactive measurement gauges for liquid or solid thicknesses (e.g., gauging of automobile sheet steel) **(DOE, 1998)**. Applications of cesium in nuclear medicine include PET imaging, tumor treatment, and measuring correct patient dosages of radiopharmaceuticals **(Adelstein and Manning, 1995)**.

3.7.1. Separation technique:

In this technique, the radiocesium is retained by the nickel ferrocyanide [nickel hexacyanoferrate(II)] complex during precipitation of this complex from an alkaline media. After separation of the formed $Fe_2O_3.nH_2O$ precipitate, the fission-products solution was transferred to another conical flask. A solution containing 30 mg sodium ferrocyanide was added to the fission-products solution dropwise with stirring to attain homogeneity. The solution was left to withstand for about 15 min. Then, a solution containing 26 mg nickel chloride was added to the fission-products solution, also, dropwise with stirring. Once more, the fission-products solution was left for about 15 min for withstanding after adding the nickel chloride solution. Final concentrations of sodium ferrocyanide and nickel chloride in the fission-products solution were 0.01 and 0.02 M,

respectively. pH-value of the solution was raised gradually and slowly, for the same reasons mentioned above with precipitation of $Fe_2O_3.nH_2O$, until it reached ~10 **(Rahman et al., 1997)** and left for one hour to settle completely the formed nickel ferrocyanide complex, $Ni_2[Fe(CN)_6]$. During its precipitation, nickel ferrocyanide complex, $Ni_2[Fe(CN)_6]$, retained cesium from the solution **(Lilga et al., 1998)** according to the reaction:

$$2CsOH + NiCl_2 + Na_4[Fe(CN)_6] \xrightarrow{pH=10} Cs_2Ni[Fe(CN)_6]\downarrow + 2NaCl + 2NaOH$$

After complete settling of the formed precipitate, the fission-products solution was withdrawn and centrifuged to ensure that it became free from any traces of the precipitated nickel ferrocyanide complex. Figure 3.21 (a and b) shows the gamma spectra of the fission-products solution before and after addition of sodium ferrocyanide solution and separation of the precipitated $Ni_2[Fe(CN)_6]$ complex. The precipitated complex was transferred semi-quantitatively from the conical flask on a Whatman No. 1 filter paper and washed with a sodium sulfate solution of pH10. Finally, the precipitate was dissolved in dilute sulfuric acid. Comparing the gamma spectra obtained in (a) and (b) of Figure 3.21 indicates disappearance of ^{134}Cs and ^{137}Cs from the fission-products solution after precipitation of nickel ferrocyanide complex.

Generally, the use of hexayanoferrate (HCF) complexes for the recovery of cesium isotopes from fission-products solution is already well established in the nuclear industry. Much work has been devoted to investigate preparation methods and properties of HCF's of many bi, tri, and tetravalent metals. HCF's of the transition metals can be prepared in either the Fe(II) or Fe(III) form, i.e., HCF(II) or HCF(III), respectiveley **(Jacobi and Streat, 1991)**. Hexacyanoferrates were selected for several

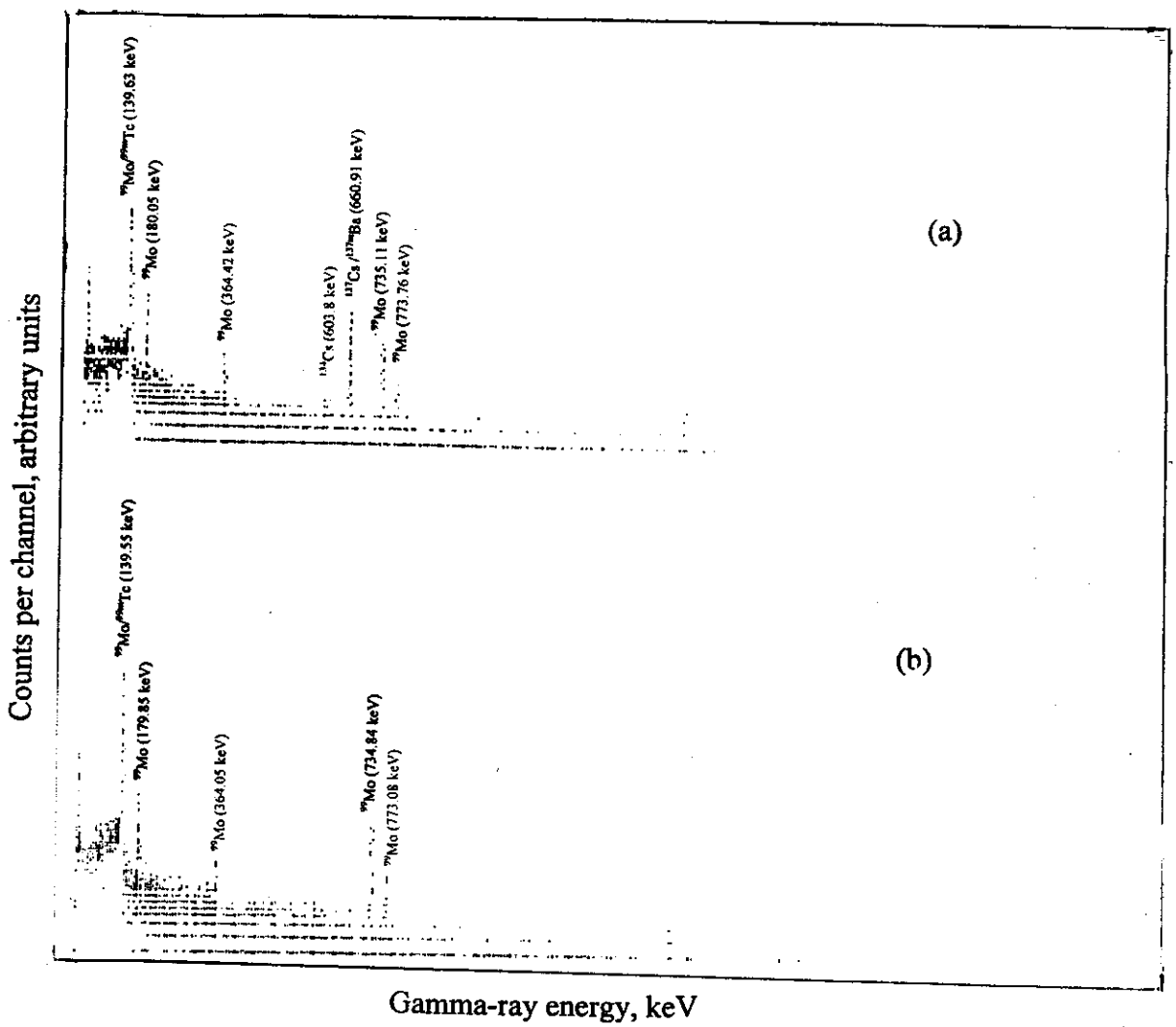

Figure 3.21. Gamma spectra of the fission-products solution (a) before addition of sodium ferrocyanide and (b) after addition of sodium ferrocyanide and nickel chloride and separation of the formed precipitate.

reasons; these are: (i) extreme selectivity for cesium in the presence of high sodium concentrations (ii) chemical and radiation stability, and (iii) simplicity and reproducibility of preparation using low-cost reagents **(Prout et al., 1965; Loewenschuss, 1982; Lehto and Harjula, 1987; Tusa et al., 1994)**.

3.7.2. Quality control of the ^{137}Cs product:

3.7.2.1. Separation and recovery yields:

Figure 3.22 (a and b) shows the gamma spectra of the nickel ferrocyanide solution (in dilute H_2SO_4) with counting times of 500 and 5000 s. As shown in Figure 3.22 (b), the isotopes ^{134}Cs, ^{136}Cs and $^{137}Cs/^{137m}Ba$ appeared in the gamma spectrum of the nickel ferrocyanide solution. Table 3.13 compiles the radiometric analysis data of the ^{134}Cs, ^{136}Cs, and ^{137}Cs radionuclides in: (i) the fission-products solution before addition of the sodium ferrocyanide solution and after separation of the formed nickel ferrocyanide precipitate, and (ii) the nickel ferrocyanide solution (in dilute H_2SO_4). It was found that precipitation of the nickel ferrocyanide complex at pH-value of 10, with concentrations of 0.01 M sodium ferrocyanide (30 mg) and 0.02 M nickel chloride (26 mg), was sufficient to remove more than 99.99 % of ^{137}Cs from the fission-products solution, i.e., separation yield of ^{137}Cs ($S_{(Cs\text{-}137)}$) was > 99.99 %. The recovery yield of ^{137}Cs, i.e, production yield ($R_{(Cs\text{-}137)}$), as defined by Equation 2.6, was found to be 98.3 %. The fraction of separated ^{137}Cs which was not detected in the nickel ferrocyanide solution (< 1.69 %) might be lost during processes of washing and dissolution of the precipitated nickel ferrocyanide complex.

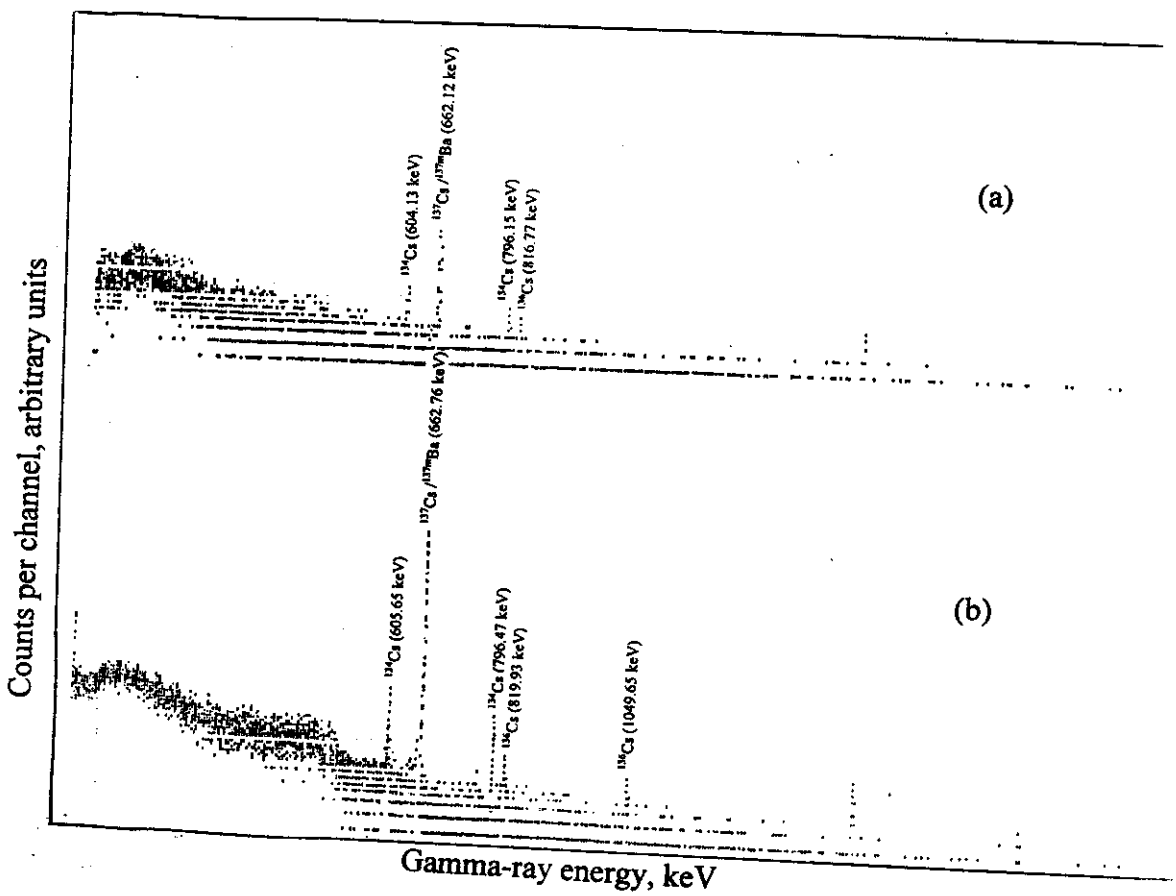

Figure 3.22. Gamma spectra of the nickel ferrocyanide solution (in dilute H_2SO_4) with counting times of (a) 500 s and (b) 5000 s.

Table 3.13. Radiometric analysis data for separation and recovery of ^{137}Cs.

Isotope			^{134}Cs	^{136}Cs	^{137}Cs	^{137m}Ba
CTRDs of the obtained γ-photopeaks in keV	F.P solution	Before addition of sodium ferrocyanide	603.8	Not detected	660.91	
		After separation of nickel ferrocyanide	Not detected	Not detected	Not detected	Not detected
	Nikel ferrocyanide solution	Counting time = 500 s	604.13, 796.15	816.77	662.12	
		Counting time=5000 s	605.65, 796.47	819.93, 1049.65	662.76	
Net area under the main γ-photopeak (normalized to the total volume of the solution)	F.P solution (countig time = 500s)	Before addition of sodium ferrocyanide	683	-	5457	
		After separation of nickel ferrocyanide	-	-	-	-
	Nikel ferrocyanide solution	Counting time =500s	981	0	5364	
		Counting time = 5000 s	9717	25	53104	

3.7.2.2. Radionuclidic purity:

According to the radiometric analysis data (Table 3.13), radionuclidic purity of the recovered ^{137}Cs, i.e., fraction of the total γ-radioactivity of the nickel ferrocyanide solution (in dilute H_2SO_4) which was contributed to $^{137}Cs/^{137m}Ba$, was 84.5 % at end of the separation process. Radionuclide contaminants of 15.46 % and 0.04 % of the total γ-radioactivity of the nickel ferrocyanide solution (in dilute H_2SO_4) were due to ^{134}Cs and ^{136}Cs, respectively. In spite of its low fission yield (Y_f = 0.0062 %), ^{136}Cs appeared in the gamma spectra shown in Figure 3.22 due to its high-abundance and high-energy gamma rays (99.7 % of 818.5 keV).

3.7.2.3. Radioactivity and specific activity:

Radioactivity of the recovered ^{137}Cs, $A_{(Cs\text{-}137)}$, was calculated according to:

$$A_{(Cs\text{-}137)} = R_{(Cs\text{-}137)alk}\ A_{0(Cs\text{-}137)} \qquad (3.4)$$

Where,

$A_{0(Cs\text{-}137)}$ = radioactivity of ^{137}Cs obtained at end of irradiation, it was calculated by using Equation (1.3).

Since ^{137}Cs is a long-lived isotope ($T_{1/2}$ = 30.17 y), the decrease in its radioactivity during nine days can be neglected, so that the term $e^{-\lambda_{(Cs\text{-}137)}t}$ was not included in Equation (3.4). For weights of 0.02, 0.06, and 0.1 g of the irradiated UO_3 targets, calculated values of $A_{(Cs\text{-}137)}$ were found to be 4, 11, and 19 μCi, respectively.

Table 3.14. Quality control data of the ^{137}Cs product.

Separation yield, $S_{(Cs\text{-}137)}$		> 99.99 %
Recovery yield, $R_{(Cs\text{-}137)}$		98.3 %
Radionuclidic purity		84.5 %
% Other radionuclides		15.46 % ^{134}Cs and 0.04 % ^{136}Cs
Calculated radioactivity, µCi	0.02 g of UO_3	4
	0.06 g of UO_3	11
	0.1 g of UO_3	19
Calculated specific activity, µCi/ml	0.02 g of UO_3	1
	0.06 g of UO_3	2
	0.1 g of UO_3	4

Specific activity of ^{137}Cs (μCi/ml) could be calculated by dividing $A_{(Cs\text{-}137)}$ by volume of the solution containing the recovered ^{137}Cs (5 ml). Thus for weights of 0.02, 0.06, and 0.1 g of the irradiated UO_3 targets, calculated specific activities of the recovered ^{137}Cs were found to be 1, 2, and 4 μCi/ml, respectively. Table 3.14 compiles the quality control data of the ^{137}Cs product.

3.8. Production of radiomolybdenum:

Figure 3.1 (b) indicates presence of the γ-photopeaks of ^{99}Mo (140.1, 181.75, 366.33, 742.29, and 781.06 keV). There are eight ^{235}U-fission molybdenum isotopes; ^{95}Mo, ^{97}Mo, ^{98}Mo, ^{99}Mo, ^{100}Mo, ^{101}Mo, ^{102}Mo, and ^{105}Mo. Of these isotopes, ^{95}Mo, ^{97}Mo, ^{98}Mo, and ^{100}Mo are stable ones. The isotopes of ^{101}Mo, ^{102}Mo, and ^{105}Mo are short-lived isotopes with half-life periods of 14.6 min, 11.3 min, and 35.6 s, respectively, so that they decayed completely during the seven-days cooling period. The latter three isotopes decay as follows:

1. ^{101}Mo decays to ^{101}Tc ($T_{1/2}$ = 14.2 min) which finally decays to stable ^{101}Ru.
2. ^{102}Mo decays to ^{102m}Tc ($T_{1/2}$ = 4.35 min) which in turn decays to ^{102}Tc ($T_{1/2}$ = 5.28 s), which finally decays to stable ^{102}Ru.
3. ^{105}Mo decays to ^{105}Tc ($T_{1/2}$ = 7.6 min) which decays to ^{105}Ru which in turn decays to ^{105}Rh, which finally decays to stable ^{105}Pd (Figure 3.19, c).

The short-lived isotopes ^{101}Tc, ^{102m}Tc, ^{102}Tc, ^{105}Tc, ^{105}Ru, and ^{105m}Rh decayed completely during the seven-days cooling period. The stable isotopes of ^{101}Ru, ^{102}Ru, and ^{104}Ru would be distilled off along with ^{103}Ru and ^{106}Ru (Section 3.4). Rhodium-105 was previously coprecipitated with $Fe_2O_3.nH_2O$ (Section 3.6.2).

Molybdenum-99 ($T_{1/2}$ = 2.75 d) is the most important fission-molybdenum isotope. The majority of ^{99}Mo (87.9 %) decays to ^{99m}Tc ($T_{1/2}$ = 6.01 h) which in turn decays to ^{99}Tc ($T_{1/2}$ = 2.13 × 10^5 y) which finally decays to stable ^{99}Ru, whereas 21.1 % of ^{99}Mo decays directly to ^{99}Tc. Figure 3.23 shows the decay chain of ^{99}Mo as a ^{235}U-fission product, while Table 3.15 compiles the nuclear characteristics and fission yields of the molybdenum and technetium isotopes produced from fission reactions of ^{235}U.

Molybdenum-99 gained its importance from its daughter ^{99m}Tc which has many important applications in nuclear medicine, where its suitable half-life and gamma energy (87.2 % of 140.51 keV) and absence of beta radioactivity play an important role in diagnostic and therapeutic purposes. About 80 % of the diagnostic nuclear medicine procedures are performed using ^{99m}Tc labeled compounds **(Nair et al., 1992)**, where they are used in both conventional γ-scanning and SPECT imaging, e.g., imaging patients with basal ganglia disease, SPECT imaging for lung cancer, cerebral SPECT imaging for Alzheimer's disease and multi-infarct dementia **(Gemmell et al.,1988; Smith et al., 1988; Takekawa et al., 1999)**. The starting material for the ^{99m}Tc-labeled compounds is sodium pertechnetate which is produced from ^{99}Mo/^{99m}Tc generators which consist of chromatographic columns loaded with ^{99}Mo and from which ^{99m}Tc is eluted with a high degree of purity **(Noronha et al., 1976; Boyd, 1987)**.

Molybdenum-99 can be produced either by ^{235}U (n,f), with a fission yield of 6.11 %, or ^{98}Mo (n,γ) reactions. In case of ^{98}Mo(n,γ) reactions, lower specific activities of ^{99}Mo are produced, which require larger chromatographic columns, and consequently lower concentrations of ^{99m}Tc (in the pertechnetate form) eluates. On the other hand, ^{235}U(n,f) reaction produces higher specific activities of ^{99}Mo, which require smaller

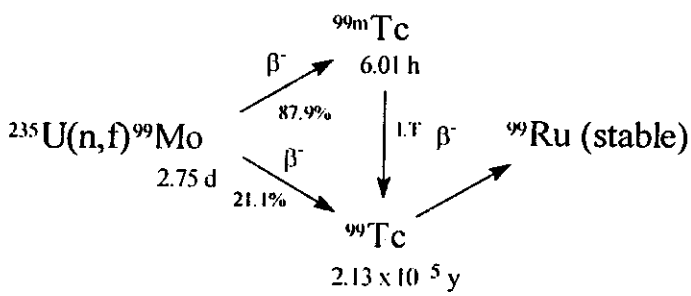

Figure 3.23. Decay chain of ^{99}Mo as a ^{235}U-fission product.

Table 3.15. Nuclear characteristics and fission yields of the ^{235}U-fission molybdenum and technetium isotopes.

Isotope		Half-life, $T_{1/2}$	Fission yield, Y_f	Decay mode	Main γ-energy (abundance), and other γ-energies in keV
Molybdenum isotopes	^{95}Mo	Stable	6.5 %	-	-
	^{97}Mo	Stable	6.2 %	-	-
	^{98}Mo	Stable	5.9 %	-	-
	^{99}Mo	2.75 d	6.11 %	β^-	140.5 (89.43 %), 181.06, 366.42, 739.5, 777.92, ...
	^{100}Mo	Stable	6.29 %	-	-
	^{101}Mo	14.6 min	5.17 %	β^-	191.98 (18.8 %), 590.87, 1012.5, ...
	^{102}Mo	11.3 min	4.28 %	β^-	211.66 (3.8 %), 148.19, 211.66, ...
	^{105}Mo	35.6 s	0.916 %	β^-	85.4 (25 %), 76.5, 147.8, ...
Technetium isotopes	^{99m}Tc	6.01 h	5.37 %	I.T, β^-	140.51 (87.2 %)
	^{99}Tc	2.13×10^5 y	6.11 %	β^-	89.65 (6×10^{-4} %)
	^{101}Tc	14.2 min	5.17 %	β^-	306.88 (88 %), 127.1, 545.11, ...
	^{102m}Tc	4.35 min	4.29 %	I.T, β^-	475.06 (87.2 %), 628.05, 1615.3, ...
	^{102}Tc	5.28 s	0.224 %	β^-	475.02 (6.7 %), 468.9, 865.5, ...
	^{105}Tc	7.6 min	0.964 %	β^-	143.2 (11 %), 107.95, 321.5, ...

chromatographic columns, and consequently produce higher concentrations of the pertechnetate eluates **(Nair et al., 1992)**.

3.8.1. Recovery of ^{99}Mo:

The processing steps of: (i) digestion of the irradiated uranium targets, (ii) separation of radioiodine, (iii) separation of radioruthenium, (iv) batch separation of Sr, Ba, La, and Ce radionuclides, (v) batch separation of Zr, Nb, Te, and Np radionuclides, and (vi) separation of radiocesium are considered as decontamination steps to recover ^{99}Mo.

After adding H_2O_2 solution (Section 3.6.1) to the fission-products solution, any reduced molybdenum species were oxidized to Mo(VI) **(El-Absy, 1991)**. The equilibrium of Mo(VI) species in aqueous solutions at different pH-values **(Mitchell, 1990; Mitchell, 1999; Aveston et al., 1964)** can be written as follows:

$$[MoO_4]^{2-} \underset{pH>6}{\overset{pH5\text{-}6}{\rightleftharpoons}} [Mo_7O_{24}]^{6-} \overset{pH3\text{-}5}{\rightleftharpoons} [Mo_8O_{26}]^{4-} \overset{pH\,1\text{-}2.9}{\rightleftharpoons} MoO_3.2H_2O\downarrow \overset{pH<0.9}{\rightleftharpoons} [MoO_2]^{2+}$$

normal molybdate — heptamolybdate — octamolybdate — hydrated molybdenum trioxide — molybdyl

According to the former equilibrium, the predominant species of Mo(VI) in the acidified fission-products solution was $[MoO_2]^{2+}$. During raising pH of the fission-products solution (Section 3.6.1), as pH value exceeded 6, $[MoO_4]^{2-}$ became the predominant species of Mo(VI) in the fission-products solution. Thus, In the final solution, after separation of radiocesium, $[MoO_4]^{2-}$ remained as the predominant species.

3.8.2. Quality control of the ^{99}Mo product:

3.8.2.1. Recovery yield:

Table 3.16 compiles the radiometric analysis data of ^{99}Mo and ^{99m}Tc in (i) the fission-products solution obtained directly after digestion of the

irradiated target and separation of the formed residue, and (ii) the final solution obtained after separation of the precipitated nickel ferrocyanide complex. According to data given in Table 3.16, it was found that recovery yield, i.e., production yield ($R_{(Mo\text{-}99)}$), of ^{99}Mo (Equation 2.7) was found to be 70.02 %.

Using the well-known equation **(Ehmann and Vance, 1991)**:

$$A / A_0 = e^{-\lambda t} \qquad (3.5)$$

where,

A_0 = radioactivity of ^{99}Mo initially present directly after digestion of the irradiated target and separation of the formed uranium-bulk residue,

A = radioactivity of ^{99}Mo that should have remained after precipitation and separation of the formed nickel ferrocyanide supposing that all the decrease in radioactivity of ^{99}Mo was only due to its decay,

λ = decay constant of ^{99}Mo (0.252 d^{-1}), and

t = time left from the moment at which radioactivity of ^{99}Mo = A_0 to that at which radioactivity of ^{99}Mo = A (t = 1.25 d),

it was found that 72.98 % of the initial ^{99}Mo radioactivity (present directly after digestion of the irradiated target and separation of the residue) should have been remained after separation of the nickel ferrocyanide precipitate, so that it can be easily deduced that 2.96 % of ^{99}Mo was lost during: (i) transferring the fission-products solution from one container to another, and (ii) the aforementioned three precipitation processes (sections 3.5, 3.6, and 3.7).

Table 3.16. Radiometric analysis data for recovery of ^{99}Mo.

Isotope		^{99}Mo	^{99m}Tc
CTRDs of the obtained γ-photopeaks in keV (F.P solution)	Directly after digestion and separation of the residue	140.87, 181.67, 365.61, 740.69, 778.4	140.87
	After separation of the nickel ferrocyanide precipitate	139.55, 179.85, 364.05, 734.84, 773.08	139.55
Net area under the main γ-photopeak in F.P solution (normalized to the total volume of the solution)	Directly after digestion and separation of the residue	8322240	
	After separation of the nickel ferrocyanide precipitate	5827319	

3.8.2.2. Radionuclidic purity:

As shown in Figure 3.21 (b), after separation of the radiocesium, only ^{99}Mo and its daughter ^{99m}Tc appeared in the gamma spectrum of the finally obtained solution and no other radionuclides were detected. Radionuclidic purity of the recovered ^{99}Mo, i.e., fraction of total γ-radioactivity of the finally obtained solution (after separation of the precipitated nickel ferrocyanide complex) which was contributed to ^{99}Mo/^{99m}Tc, was found to be > 99.9 %.

3.8.2.3. pH-value of the product solution:

pH-value of the final solution obtained after separation of the precipitated nickel ferrocyanide complex was found to be 10.

3.8.2.4. Radioactivity and specific activity:

Radioactivity of the recovered ^{99}Mo, $A_{(Mo\text{-}99)}$, was calculated according to:

$$A_{(Mo\text{-}99)} = R_{(Mo\text{-}99)} A_{0(Mo\text{-}99)} \qquad (3.6)$$

Where,

$A_{0(Mo\text{-}99)}$ = radioactivity of ^{99}Mo obtained at end of irradiation, it was calculated by using Equation (1.3).

For weights of 0.02, 0.06, and 0.1 g of the irradiated UO_3 targets, calculated values of $A_{(Mo\text{-}99)}$ were found to be 1368, 4104, and 6841 μCi, respectively.

Specific activity of ^{99}Mo (μCi/ml) could be calculated by dividing $A_{(Mo\text{-}99)}$ by volume of the final solution containing the recovered ^{99}Mo (10 ml). Thus for weights of 0.02, 0.06, and 0.1 g of the irradiated UO_3 targets, calculated specific activities of the recovered ^{99}Mo were found to

be 137, 410, and 684 μCi/ml, respectively. Table 3.17 compiles the quality control data of the ^{99}Mo product.

Figure 3.24 illustrates flow-chart of the production process of ^{131}I, ^{103}Ru, ^{137}Cs, and ^{99}Mo from ^{235}U-fission reaction including batch separation of two groups of elements; (i) Sr, Ba, La, and Ce, and (ii) Zr, Nb, Rh, Te, and Np.

Table 3.17. Quality control data of the ^{99}Mo product.

Recovery yield, $R_{(Mo-99)}$		70.02 %
Radionuclidic purity		> 99.9 %
pH-value		10
Calculated radioactivity, µCi	0.02 g of UO_3	1368
	0.06 g of UO_3	4104
	0.1 g of UO_3	6841
Calculated specific activity, µCi/ml	0.02 g of UO_3	137
	0.06 g of UO_3	410
	0.1 g of UO_3	684

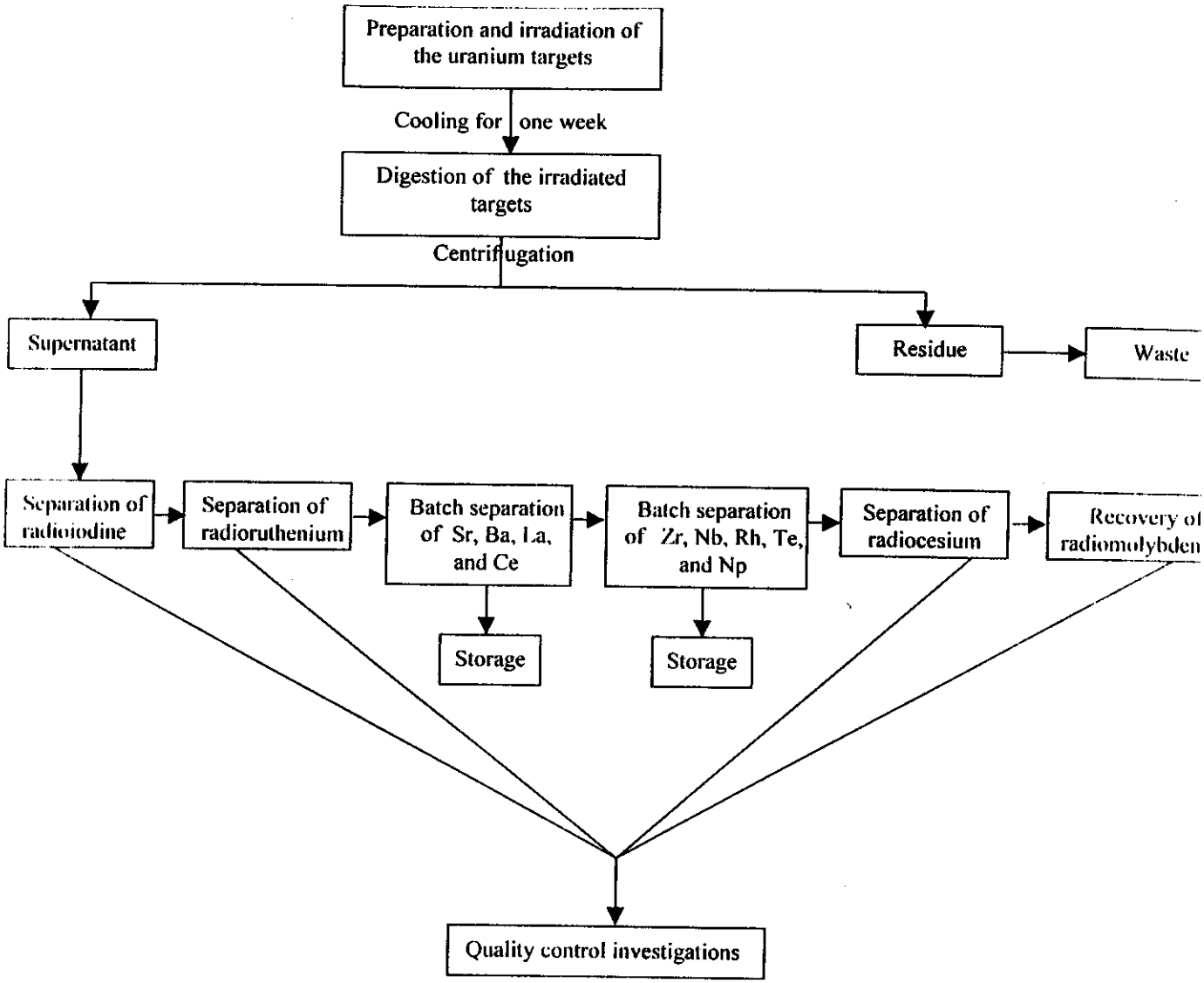

Figure 3.24. Sequential separation flow-chart of the ^{235}U-fission products: ^{131}I, ^{103}Ru, ^{137}Cs, and ^{99}Mo radionuclides.